



**NAVAL
POSTGRADUATE
SCHOOL**

MONTEREY, CALIFORNIA

THESIS

**REDUCING THE SURFACE PERFORMANCE
REQUIREMENTS OF A PRIMARY MIRROR BY
ADDING A DEFORMABLE MIRROR IN ITS OPTICAL
PATH**

by

Ernesto R. Villalba

December 2015

Thesis Advisor:

Brij Agrawal

Co-Advisor:

Jae Jun Kim

Approved for public release; distribution is unlimited

THIS PAGE INTENTIONALLY LEFT BLANK

REPORT DOCUMENTATION PAGE			<i>Form Approved OMB No. 0704-0188</i>	
Public reporting burden for this collection of information is estimated to average 1 hour per response, including the time for reviewing instruction, searching existing data sources, gathering and maintaining the data needed, and completing and reviewing the collection of information. Send comments regarding this burden estimate or any other aspect of this collection of information, including suggestions for reducing this burden, to Washington headquarters Services, Directorate for Information Operations and Reports, 1215 Jefferson Davis Highway, Suite 1204, Arlington, VA 22202-4302, and to the Office of Management and Budget, Paperwork Reduction Project (0704-0188) Washington, DC 20503.				
1. AGENCY USE ONLY (Leave blank)		2. REPORT DATE December 2015	3. REPORT TYPE AND DATES COVERED Master's thesis	
4. TITLE AND SUBTITLE REDUCING THE SURFACE PERFORMANCE REQUIREMENTS OF A PRIMARY MIRROR BY ADDING A DEFORMABLE MIRROR IN ITS OPTICAL PATH			5. FUNDING NUMBERS	
6. AUTHOR(S) Ernesto R. Villalba				
7. PERFORMING ORGANIZATION NAME(S) AND ADDRESS(ES) Naval Postgraduate School Monterey, CA 93943-5000			8. PERFORMING ORGANIZATION REPORT NUMBER	
9. SPONSORING /MONITORING AGENCY NAME(S) AND ADDRESS(ES) N/A			10. SPONSORING/MONITORING AGENCY REPORT NUMBER	
11. SUPPLEMENTARY NOTES The views expressed in this thesis are those of the author and do not reflect the official policy or position of the Department of Defense or the U.S. government. IRB Protocol number <u> N/A </u> .				
12a. DISTRIBUTION / AVAILABILITY STATEMENT Approved for public release; distribution is unlimited			12b. DISTRIBUTION CODE	
13. ABSTRACT (maximum 200 words) In recent years, carbon fiber reinforced polymer (CFRP) mirrors been proposed for use in future imaging satellites. Compared to traditional glass-based mirrors, CFRP mirrors offer reduced manufacturing times, lower coefficients of thermal expansion, lower areal density, and higher strength-to-weight ratios. Shorter manufacturing times promise to reduce program schedule requirements and cost. These advantages come at the expense of surface quality, which results in wavefront errors that are outside of the diffraction limit for optical imaging. To compensate for the reduced surface quality of CFRP mirrors, a deformable mirror (DM) is required in the optical path. During this research, the surface quality of a CFRP mirror was evaluated to establish a root-mean-square (RMS) error threshold for the DM corrections. An integral DM control law that employed a constrained least-squares solution was utilized to reduce the overall system wavefront error to below the specified CFRP error threshold. The application of this control law yielded a 38% reduction in RMS wavefront error (as compared to the CFRP error threshold), thus reducing the CFRP RMS surface performance requirements by the same amount. Reducing the surface performance requirements of CFRP mirrors is a critical step toward employing these mirrors in future imaging satellites.				
14. SUBJECT TERMS carbon fiber reinforced polymer mirror, adaptive optics, deformable mirror, surface figure error			15. NUMBER OF PAGES 79	
			16. PRICE CODE	
17. SECURITY CLASSIFICATION OF REPORT Unclassified	18. SECURITY CLASSIFICATION OF THIS PAGE Unclassified	19. SECURITY CLASSIFICATION OF ABSTRACT Unclassified	20. LIMITATION OF ABSTRACT UU	

THIS PAGE INTENTIONALLY LEFT BLANK

Approved for public release; distribution is unlimited

**REDUCING THE SURFACE PERFORMANCE REQUIREMENTS OF A
PRIMARY MIRROR BY ADDING A DEFORMABLE MIRROR IN ITS
OPTICAL PATH**

Ernesto R. Villalba
Lieutenant Commander, United States Navy
B.S., United States Naval Academy, 2004

Submitted in partial fulfillment of the
requirements for the degree of

MASTER OF SCIENCE IN ASTRONAUTICAL ENGINEERING

from the

**NAVAL POSTGRADUATE SCHOOL
December 2015**

Author: Ernesto R. Villalba

Approved by: Brij Agrawal
Thesis Advisor

Jae Jun Kim
Co-Advisor

Garth Hobson
Chair, Department of Mechanical and Aerospace Engineering

THIS PAGE INTENTIONALLY LEFT BLANK

ABSTRACT

In recent years, carbon fiber reinforced polymer (CFRP) mirrors been proposed for use in future imaging satellites. Compared to traditional glass-based mirrors, CFRP mirrors offer reduced manufacturing times, lower coefficients of thermal expansion, lower areal density, and higher strength-to-weight ratios. Shorter manufacturing times promise to reduce program schedule requirements and cost. These advantages come at the expense of surface quality, which results in wavefront errors that are outside of the diffraction limit for optical imaging. To compensate for the reduced surface quality of CFRP mirrors, a deformable mirror (DM) is required in the optical path. During this research, the surface quality of a CFRP mirror was evaluated to establish a root-mean-square (RMS) error threshold for the DM corrections. An integral DM control law that employed a constrained least-squares solution was utilized to reduce the overall system wavefront error to below the specified CFRP error threshold. The application of this control law yielded a 38% reduction in RMS wavefront error (as compared to the CFRP error threshold), thus reducing the CFRP RMS surface performance requirements by the same amount. Reducing the surface performance requirements of CFRP mirrors is a critical step toward employing these mirrors in future imaging satellites.

THIS PAGE INTENTIONALLY LEFT BLANK

TABLE OF CONTENTS

I.	INTRODUCTION.....	1
A.	MOTIVATION	1
B.	OBJECTIVES	1
C.	OVERVIEW	2
II.	BACKGROUND	3
A.	CFRP MIRROR OVERVIEW	3
B.	ADAPTIVE OPTICS OVERVIEW	4
1.	Optical Aberrations	6
2.	Deformable Mirrors.....	7
3.	Wavefront Sensors	11
C.	PREVIOUS WORK.....	13
III.	CFRP MIRROR AND DM SURFACE CHARACTERIZATION	15
A.	EXPERIMENTAL SETUP	15
B.	CFRP MIRROR SURFACE ERROR CHARACTERIZATION	19
C.	DM BASELINE SURFACE.....	21
D.	AO SYSTEM BASELINE ERROR	24
IV.	CONTROL METHOD	27
A.	INFLUENCE MATRIX COLLECTION	29
B.	LINEAR LEAST-SQUARES CONTROL	33
C.	CONTROL SCRIPT IMPLEMENTATION	36
V.	CFRP MIRROR SURFACE ERROR CORRECTION	39
A.	SIMULATED CFRP MIRROR CORRECTION	39
B.	EXPERIMENTAL CFRP MIRROR CORRECTION.....	41
VI.	CONCLUSION AND FUTURE WORK	45
A.	REDUCTION IN CFRP SURFACE PERFORMANCE REQUIREMENTS.....	45
B.	FUTURE WORK.....	45
1.	CFRP Mirror Suitability for the Space Environment.....	45
2.	Imaging Satellite AO System Implementation	45
	APPENDIX: MATLAB CODE	47
A.	CFRP ERROR CORRECTION SIMULATION MATLAB CODE.....	47
B.	CFRP ERROR CORRECTION EXPERIMENTAL MATLAB CODE	50
	LIST OF REFERENCES.....	59
	INITIAL DISTRIBUTION LIST	61

THIS PAGE INTENTIONALLY LEFT BLANK

LIST OF FIGURES

Figure 1.	1 Meter CFRP Mirror at NPS	4
Figure 2.	CFRP Cell-Type Core Structure and Facesheet.....	4
Figure 3.	Notional Spaced-Based AO System	5
Figure 4.	AOX 349 Actuator DM at NPS	9
Figure 5.	AOX DM Actuator Layout	10
Figure 6.	WinHVA Software Package	11
Figure 7.	Zygo GPI XPHR Laser Interferometer at NPS.....	12
Figure 8.	MetroPro Software Package	13
Figure 9.	1-meter CFRP Mirror Optical Layout.....	16
Figure 10.	1-meter CFRP Mirror Optical Layout Schematic.....	17
Figure 11.	Experimental Workstation Layout.....	18
Figure 12.	Experimental Workstation Schematic.....	18
Figure 13.	CFRP Baseline Error with No Masking.....	20
Figure 14.	CFRP Baseline Error with Mask Applied.....	21
Figure 15.	AOX DM Baseline Wavefront Error	22
Figure 16.	AOX DM Actuator Layout—Inoperable Actuators Highlighted	23
Figure 17.	AOX DM Baseline Image with Mask Applied.....	23
Figure 18.	Typical Baseline AO System Wavefront Error	25
Figure 19.	Schematic of Experimental AO Control System	27
Figure 20.	Schematic of Simulated AO Control System.....	29
Figure 21.	Wavefront Influence of Actuator 70	30
Figure 22.	Singular Values of the Initial Influence Matrix	31
Figure 23.	Singular Values of the Reduced Influence Matrix.....	32
Figure 24.	AOX DM Actuator Evaluation	33
Figure 25.	CFRP Error Correction Simulation Results.....	40
Figure 26.	CFRP Error Correction Experimental Results.....	42
Figure 27.	DM Control Voltage for Experimental CFRP Correction	42
Figure 28.	Data Dropout Comparison	43
Figure 29.	CFRP Error Correction with Faulty Actuators Masked.....	44

THIS PAGE INTENTIONALLY LEFT BLANK

LIST OF TABLES

Table 1.	DMN349PMN5 Physical Properties.....	9
Table 2.	Zygo GPI XPHR Laser Interferometer Specifications	12
Table 3.	Summary of CFRP RMS and PV Error Values	21
Table 4.	Summary of DM RMS and PV Error Values	24
Table 5.	Summary of CFRP Error Correction Simulation Results.....	41
Table 6.	Summary of CFRP Error Correction Experimental Results.....	44

THIS PAGE INTENTIONALLY LEFT BLANK

LIST OF ACRONYMS AND ABBREVIATIONS

2-D FFT	2-dimensional fast Fourier transform
AO	adaptive optics
AOCOE	Adaptive Optics Center of Excellence
AOX	Adaptive Optics Associates/Xinetics
CFRP	carbon fiber reinforced polymer
CSV	comma separated values
DM	deformable mirror
OST	optical surface transfer
PC	personal computer
PI	proportional-integral
PV	peak-to-valley
RMS	root-mean-square
SMT	Segmented Mirror Telescope
TCP/IP	transmission control protocol/Internet protocol
WinHVA	Windows High Voltage Amplifier

THIS PAGE INTENTIONALLY LEFT BLANK

ACKNOWLEDGMENTS

I would like to offer thanks and appreciation for the technical input and guidance my thesis advisors, Professors Brij. Agrawal and Jae Jun Kim, have provided me during the course of this thesis. In addition, I would like to offer thanks to Lt. Col. Matt Allen, Dr. Bautista Fernandez, Dr. John Bagnasco, Mr. Albert Jordan and MIDN Nick D'Antonio for the technical assistance and expertise they provided me during the experimental portion of this thesis. The work performed in this thesis would have not been possible without the help provided by my advisors and the technical staff at the Adaptive Optics Center of Excellence (AOCOE) at Naval Postgraduate School (NPS).

To my family, especially to my wife, Roxana, I offer my deepest thanks and love for all the support and encouragement I have received over the past two and a half years. My family has allowed me to spend many weekend mornings and late nights working on this thesis, and without their support, I would have not been able to complete my schoolwork at NPS.

THIS PAGE INTENTIONALLY LEFT BLANK

I. INTRODUCTION

A. MOTIVATION

In an attempt to reduce the development costs of primary mirrors in imaging satellites, replicated carbon fiber reinforced polymer (CFRP) mirrors have been proposed as a cost-effective replacement for traditional glass-based primary mirrors [1]. The reduced development costs result from the CFRP mirror manufacturing procedure, which utilizes a replication process that takes considerably less time than the traditional glass mirror manufacturing process [1], [2]. In addition, CFRP mirrors offer lower areal density, lower coefficients of thermal expansion and a higher strength-to-weight ratio as compared to glass mirrors [1], [3]. These mechanical qualities also make them a viable option for large aperture satellite systems [4]. The reduction in development costs offered by CFRP mirrors come at the expense of surface quality, which result in wavefront errors that are outside the diffraction limit for imaging [5]. For diffraction limited imaging, mirror surface root-mean-square (RMS) error requirements are typically $\lambda/15$, where λ is the wavelength of the incoming light [5]. To enable diffraction limited imaging, replicated CFRP mirrors will need to be employed with a deformable mirror (DM) in their optical path [5]. The DM will change its shape to compensate for the CFRP surface errors, thus reducing the wavefront errors to within diffraction limits [6]. The addition of a DM into the optical path will reduce the surface performance requirements of the primary mirror, thus enabling the utilization of replicated CFRP mirrors as the primary optic in imaging satellites.

B. OBJECTIVES

The main objective of this thesis is to experimentally demonstrate the reduction of the surface performance requirements of a CFRP primary mirror. This reduction will be accomplished by adding a DM in the primary mirror's optical path.

C. OVERVIEW

Chapter II will provide background information on CFRP mirror technology, adaptive optics (AO) systems, and the 349 actuator DM utilized in this thesis. Chapter III will provide details on individual CFRP mirror and DM surface characteristics. The CFRP mirror surface characterization will include the masking techniques used to eliminate and/or compensate for CFRP manufacturing defects. The DM characterization section will evaluate the mirror's unpowered baseline surface. In addition, the total system wavefront error will be evaluated. Chapter IV will cover the control method utilized to correct the wavefront errors induced by the CFRP mirror. Simulated and experimental results of the CFRP wavefront correction techniques will be presented in Chapter V. Finally, thesis conclusions and recommendations for future work will be presented in Chapter VI.

II. BACKGROUND

A. CFRP MIRROR OVERVIEW

CFRP mirrors are lightweight optics produced via a replication process called optical surface transfer (OST) [2]. The OST process transfers the optical characteristics of an optical forming mold to the CFRP material placed over the mold [2]. Once the CFRP material is released from the mold, it is ready to receive the desired optical coating, as it requires no additional polishing or processing [2]. The optical forming mold is referred to as a mandrel, and can be utilized to generate multiple replicated CFRP optics [7]. As a result of the OST process, CFRP manufacturing times are in the order of weeks, vice years for traditional glass mirrors [8]. This reduction in manufacturing time reduces program scheduling requirements, which leads to a reduction in overall program development costs. In addition to the reduction in manufacturing time, CFRP mirrors offer increased thermal stability and decreased areal density (density per unit area) [3]. Increased thermal stability enables CFRP mirror quality and optical alignment to remain stable during the high temperature fluctuations that occur during the satellite's orbit. The reduced areal density of the CFRP mirror will decrease the overall mass of the satellite's optical system, thus reducing the overall mass of the satellite. Since launch vehicle costs are directly related to the mass of the client satellite, the reduced areal density of CFRP mirrors will result in decreased launch vehicle costs. All these advantages come at the expense of surface quality, which is only as good as the surface quality of the mandrel [2]. Surface quality is also affected by the fiber and/or backing structure print-through that arise during the OST manufacturing process [5], [8]. For these reasons, the use of a DM in the mirror's optical path is required for diffraction limited imaging.

The CFRP mirror utilized in this thesis is a 1-meter parabolic aperture that was delivered to NPS in April 2015. The mirror consists of a cell-type core structure and a CFRP facesheet [4]. The facesheet acts as the mirror surface and is treated with an aluminum optical coating that enables the mirror's utilization of the visual spectrum. A visual depiction of the CFRP mirror is presented in Figure 2. Figure 3 presents the cell-type core structure and the CFRP facesheet.

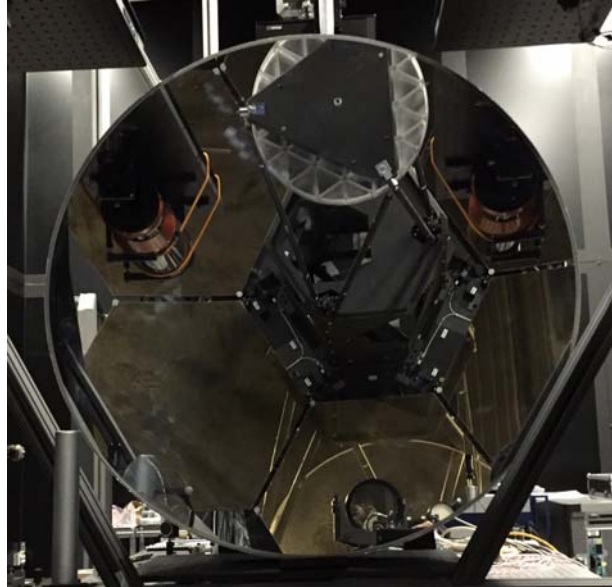


Figure 1. 1 Meter CFRP Mirror at NPS



Figure 2. CFRP Cell-Type Core Structure and Facesheet

Source: [4] J. J. Kim, M. Allen and B. Agrawal, "Cost-effective aperture with deformable mirror for imaging satellites," presented at the 66th International Astronautical Congress, Jerusalem, Israel, 2015.

B. ADAPTIVE OPTICS OVERVIEW

AO systems have been used for many years on ground based astronomical telescopes to correct for optical aberrations induced by Earth's atmosphere [6]. The adaptation of this technology to space based telescopes has been in development in recent

years, with the goal of correcting for mirror defects instead of atmospheric aberrations. A notional space-based AO system is presented in Figure 3.

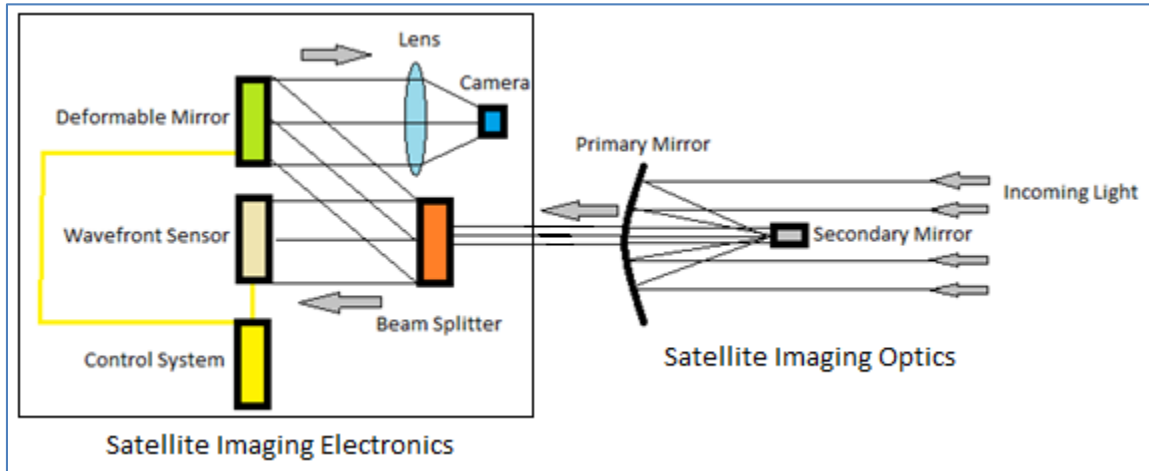


Figure 3. Notional Spaced-Based AO System

Figure 3 shows incoming light being reflected from a satellite’s imaging optics to its imaging electronics. As the incoming light is reflected by the primary mirror, aberrations are induced by imperfections on the mirror surface. These imperfections manifest themselves as “wavefront errors” that are detected by a wavefront sensor in the imaging electronics. If the mirror surface is perfect, then the reflected wavefront of the incoming light is flat and no errors are detected by the sensor [6]. The wavefront errors are passed to a control system that calculates the required input to the DM [6]. In order to correct the wavefront, the DM must deform to match the incoming aberrations [6]. Hence, the goal of the control system is to determine which shape (based on the capabilities and limitations of the DM) results in the greatest reduction in wavefront error.

In this thesis, the AO system will consist of a primary optic, a DM system, a wavefront sensor and two personal computers (PCs). The primary optic will be a 1 meter diameter CFRP mirror. The DM system will be a 349 actuator deformable mirror (and associated electronics) manufactured by Adaptive Optics Associates/Xinetics (AOX) Corporation. The wavefront sensor will be a laser interferometer built by the Zygo

Corporation (model GPI XPHR). The wavefront sensor will be connected to a Dell OPTIPLEX 7010 PC running the MetroPro software package, which allows for the gathering and processing of the interferometer data. This PC will be referred to as the “Zygo” PC. A Dell Precision T5500 PC will be utilized to command the Zygo interferometer and to generate the DM control commands. The DM control commands will be generated in the T5500 PC by utilizing a MATLAB control script. This computer will be referred to as the “Control” PC.

1. Optical Aberrations

Historically, AO techniques have been used in astronomy to correct for optical aberrations induced by atmospheric turbulence [6]. In this thesis, the concepts of AO were utilized to correct for the optical aberrations induced by the surface figure errors of a CFRP mirror. In optics, optical aberrations are typically characterized by their RMS and peak-to-valley (PV) error values in either nanometers (nm) or waves. Waves are defined as the ratio between the error value of the optical aberration and the wavelength of the incoming light. These units are used to characterize optical aberrations independent of the source wavelength. In this thesis, RMS and PV error values will be presented in waves. RMS error represents the total spread of error values around a specified threshold. In AO, the threshold is zero waves since an aberration-free wavefront has zero error values. PV error values represent the distance between maximum and minimum wavefront error value, which gives an indication of the maximum strength of the optical aberration. Equations 2.1 and 2.2 present the mathematical calculations for RMS and PV error, respectively.

$$RMS_e = \sqrt{\frac{\sum_{i=1}^N (\phi_{e_i})^2}{N}} = \frac{\|\phi_e\|_2}{\sqrt{N}} \quad (2.1)$$

$$PV_{Max} = \phi_{e_{Max}} - \phi_{e_{Min}} \quad (2.2)$$

In Equation 2.1, the term ϕ_{e_i} refers to the i^{th} wavefront error measurement out of a total of N error measurements. The term $\|\phi_e\|_2$ represents the 2-norm of the wavefront error vector. In Equation 2.2, the terms $\phi_{e_{Max}}$ and $\phi_{e_{Min}}$ refer to the maximum and minimum valued error measurements. The RMS error calculation gives a better representation of the overall wavefront aberration in comparison to the PV error calculation since the PV calculation gives the difference between maximum and minimum error values without characterizing the distribution of the aberrations throughout the wavefront [9], [10]. Hence, the primary metric for characterizing the initial and residual (after DM correction) optical aberrations was RMS error in waves. The percent reduction in RMS error was calculated by comparing the initial and residual RMS error values. Equation 2.3 shows the RMS percent reduction calculation. A similar calculation was performed to compare initial and residual PV values. Since mirror surface performance requirements are typically given in RMS, a reduction in RMS error is directly proportional to a reduction in surface performance requirements.

$$RMS_{\%R} = \frac{RMS_{initial} - RMS_{residual}}{RMS_{initial}} \times (100) \quad (2.3)$$

2. Deformable Mirrors

A DM is an optical instrument that changes the physical shape of its reflective surface in a manner that counteracts the aberrations of the incoming light it reflects [6]. DM's are characterized by the type of reflective surface and by the number and type of actuators. There are 2 types of reflective surfaces: continuous and segmented. Segmented surfaces offer no cross-coupling between actuators, but the discontinuities (gaps) in the segmented surface result in decreased system performance since the incoming light is diffracted by the gaps [6]. Continuous reflective surfaces do not suffer from this energy loss due to refraction. For this thesis, a continuous surface DM was utilized. Continuous surface DM's are typically implemented with discrete type actuators that are attached

perpendicularly to the back of the DM surface [6]. These actuators provide a positive or negative force perpendicular to the DM surface that is utilized to deform the DM surface into a desired shape. The number of actuators within the DM aperture dictates the spatial resolution of the DM [5]. The required number of DM actuators is directly proportional to the spatial frequency of the aberration to be corrected [5]. Another important DM parameter is the actuator stroke. The required actuator stroke (range of motion of each actuator) is directly proportional to the strength (typically measured in wavelengths) of the aberration to be corrected [11]. Typical DM actuator strokes range from 3 to 4 micrometers [11]. In this thesis, an AOX continuous surface (349 discrete actuator, 4 micrometer stroke) DM was utilized. This DM was selected since it was the most capable DM (in terms of number of actuators and stroke) available at NPS. Detailed information on the AOX 349 actuator DM is provided in the next paragraph.

The AOX 349 actuator DM, model number DM349PMN5, was utilized to reduce the surface performance requirements of the 1 meter CFRP mirror at NPS. The AOX DM system includes the DM and an electronics rack [12]. The electronics rack houses a Windows PC, 11 electronics boards, a fan assembly, and other associated electronics [12]. The PC (through the 11 electronics boards) controls the performance of all 349 actuators [12]. This PC will be referred to as the “AOX DM” PC. The AOX DM is depicted in Figure 4.

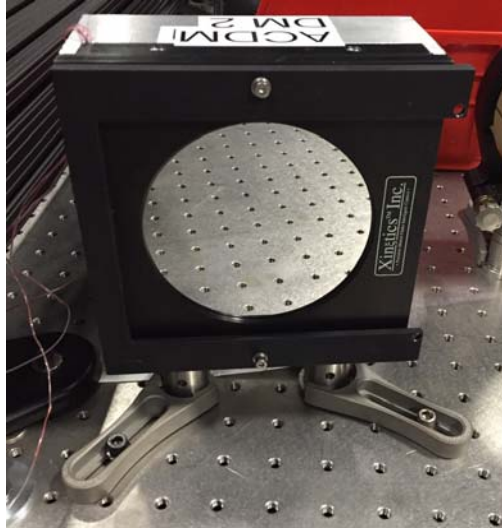


Figure 4. AOX 349 Actuator DM at NPS

As depicted in Figure 4, the DM has a circular continuous surface aperture that is made of ultra-low expansion (ULE) glass [13]. A summary of the main physical properties of this DM is presented in Table 1.

Table 1. DMN349PMN5 Physical Properties

DM Parameter	Value
Mirror Composition	ULE Glass
Mirror Coating	Protected Silver
Aperture Diameter	100 mm
Mirror Thickness	2 mm
Number of Actuators	349
Actuator Material	Lead Manganese Niobate (PMN)
Actuator Pitch (Separation)	5 mm
Maximum Actuator Stroke	4 μ m
Input Voltage Range	\pm 30 V
Actuator Coupling	10 % between adjacent actuators

Adapted from: [13] B. R. Oppenheimer, D. L. Palmer, R. G. Dekany, A. Sivaramakrishnan, M. A. Ealey and T. R. Price, "Investigating a Xinetics Inc. Deformable Mirror," *SPIE*, vol. 3126, pp. 569–579, 1997; [14] Surface Normal Mirrors. (n.d.). Northrup Grumman. [Online]. Available: <http://www.northropgrumman.com/BusinessVentures/AOAXinetics/IntelligentOptics/Products/Pages/SurfaceNormalMirrors.aspx>.

The DM's 349 actuators are arranged in a 21 row by 21 column configuration that approximates a circular aperture. This configuration is presented in Figure 5. The actuators are controlled by a Windows PC running the Windows High Voltage Amplifier (WinHVA) software package. The WinHVA software is capable of commanding individual actuators or all 349 actuators simultaneously [15]. To command all 349 actuators simultaneously, the user must load a comma separated value (CSV) command map into the WinHVA software [15]. The command map is composed of actuator count values that correspond to a desired actuator voltage [15]. For the allowed actuator voltage range of ± 30 V, the command count range is -2048 to 2047 [15]. A visual depiction of the WinHVA software is presented in Figure 6.

										1	2	3	4	5	6	7														
										8	9	10	11	12	13	14	15	16	17	18										
										19	20	21	22	23	24	25	26	27	28	29	30	31								
										32	33	34	35	36	37	38	39	40	41	42	43	44	45	46						
										47	48	49	50	51	52	53	54	55	56	57	58	59	60	61	62	63				
										64	65	66	67	68	69	70	71	72	73	74	75	76	77	78	79	80	81	82		
										83	84	85	86	87	88	89	90	91	92	93	94	95	96	97	98	99	100	101		
										102	103	104	105	106	107	108	109	110	111	112	113	114	115	116	117	118	119	120	121	122
										123	124	125	126	127	128	129	130	131	132	133	134	135	136	137	138	139	140	141	142	143
										144	145	146	147	148	149	150	151	152	153	154	155	156	157	158	159	160	161	162	163	164
										165	166	167	168	169	170	171	172	173	174	175	176	177	178	179	180	181	182	183	184	185
										186	187	188	189	190	191	192	193	194	195	196	197	198	199	200	201	202	203	204	205	206
										207	208	209	210	211	212	213	214	215	216	217	218	219	220	221	222	223	224	225	226	227
										228	229	230	231	232	233	234	235	236	237	238	239	240	241	242	243	244	245	246	247	248
										249	250	251	252	253	254	255	256	257	258	259	260	261	262	263	264	265	266	267		
										268	269	270	271	272	273	274	275	276	277	278	279	280	281	282	283	284	285	286		
										287	288	289	290	291	292	293	294	295	296	297	298	299	300	301	302	303				
										304	305	306	307	308	309	310	311	312	313	314	315	316	317	318						
										319	320	321	322	323	324	325	326	327	328	329	330	331								
										332	333	334	335	336	337	338	339	340	341	342										
										343	344	345	346	347	348	349														

Figure 5. AOX DM Actuator Layout

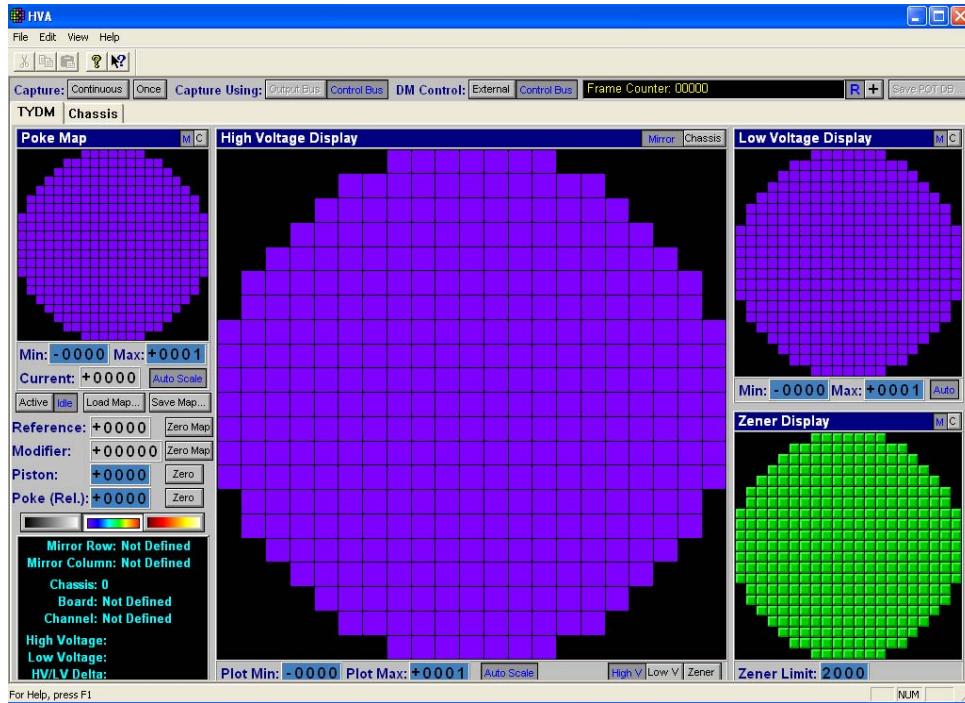


Figure 6. WinHVA Software Package

3. Wavefront Sensors

The wavefront sensor is a major component of the AO system. The sensor provides wavefront error data to the control computer, which utilizes the sensor data to generate the required DM control commands. Once the control commands are sent to the DM, the sensor takes another measurement. This process is repeated until the wavefront error is within a desired limit. The work performed in this thesis utilized a laser phase-shifting interferometer as the wavefront sensor. A detailed description of this sensor is provided in the next paragraph.

A Zygo laser interferometer, model GPI XPHR, was the wavefront sensor utilized to reduce the surface performance requirements of the 1 meter CFRP mirror at NPS. The interferometer system consists of a phase-shifting laser interferometer and a Dell OPTIPLEX 7010 Windows PC running the MetroPro software package. A depiction of the Zygo laser interferometer is presented in Figure 7. A summary of the interferometer's main technical specifications is presented in Table 2.

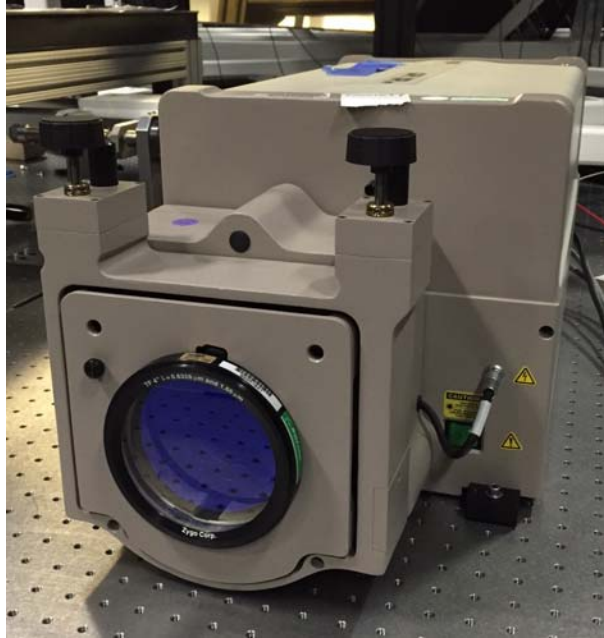


Figure 7. Zygo GPI XPHR Laser Interferometer at NPS

Table 2. Zygo GPI XPHR Laser Interferometer Specifications

Parameter	Value
Laser Type	Helium-Neon, Class II
Laser Wavelength	632.8 nm
Spatial Sampling	Low Resolution: 320 x 240 pixels High Resolution: 640 x 320 pixels
Measurement Resolution	$\lambda/8000$ waves
Data Acquisition Time	Low Resolution: 140 ms High Resolution: 260 ms

Adapted from [16] GPI XP, GPI XPHR, GPI HS specifications. (n.d.). Zygo Corporation. [Online]. Available: http://www.lambdaphoto.co.uk/pdfs/GPI_xp_spec.pdf.

The Zygo laser interferometer features a high-resolution/high-speed camera that provides a 3-dimensional depiction of the measured wavefront error. The measured error data is provided in either waves or nm. The interferometer is commanded via the MetroPro software package, which is also capable of analyzing the collected sensor data. During this thesis work, the MetroPro software (in conjunction with a MATLAB script)

was utilized to generate wavefront RMS and PV error values. A visual depiction of the MetroPro software is presented in Figure 8.

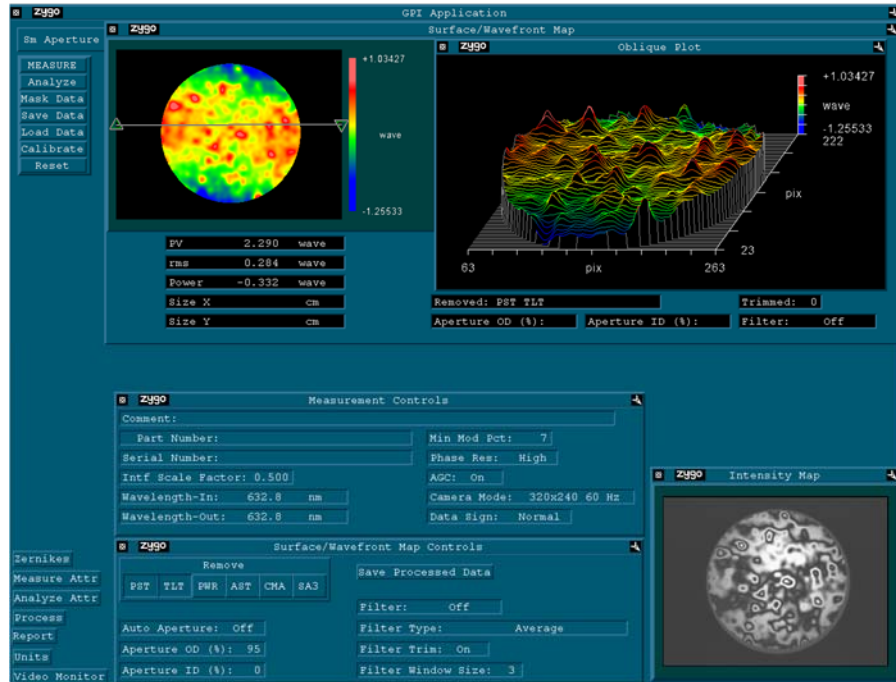


Figure 8. MetroPro Software Package

C. PREVIOUS WORK

In his 2007 master's thesis, Allen [17] examined various techniques for controlling a DM. The techniques included an iterative proportional-integral (PI) control method that experimentally demonstrated the correction of laser light aberrations with a DM [17]. Following the work performed by Allen in 2007, Watson's 2013 master's thesis [18] examined various techniques for controlling a DM to compensate for the surface figure errors present in one of the primary mirror segments of the Segmented Mirror Telescope (SMT) at NPS. Watson utilized manual control and iterative PI least-squares (unconstrained and constrained) control techniques to correct surface figure errors [18]. Utilizing iterative PI constrained least-squares control, Watson demonstrated a 55% RMS improvement in the surface figure of an SMT primary mirror segment [18]. Based on the work performed by Allen and Watson, this thesis will evaluate an integral

control technique that employs a constrained least-squares solution for correcting the surface figure errors present in the CFRP mirror at NPS.

III. CFRP MIRROR AND DM SURFACE CHARACTERIZATION

In this chapter, the surface characteristics of both the CFRP mirror and the AOX DM will be evaluated. First, the baseline surface figure error of the CFRP mirror without a DM in the optical path will be established. The results from DM control simulations and experiments (presented in the next chapter) will be compared against this CFRP baseline. Next, the AOX DM surface figure error will be established since the total error of the AO system includes both CFRP and DM surface figure errors. For the AO system to be successful, it must correct the total wavefront error of the system (induced by a combination of CFRP and DM surface errors) to a level below the CFRP baseline error. For this reason, the total AO system wavefront error will be characterized in the last section of this chapter.

A. EXPERIMENTAL SETUP

The experimental portions of this thesis were conducted at the SMT Laboratory at NPS. The laboratory housed the 1-meter CFRP mirror and the AOX DM in an air-floating table that rejects vibrations from the ground. Figure 9 shows the CFRP optical layout within the SMT laboratory. A detailed schematic of the CFRP optical layout is presented in Figure 10. As presented in Figure 10, the initial experimental setup utilized a flat mirror instead of a DM. This was done to collect the CFRP baseline data. Once this data was collected, the DM was placed in the optical path of the CFRP. The DM surface figure data was collected by implementing a flip mirror (as depicted in Figure 10) in the optical path between the CFRP and the DM. With the flip mirror in the UP position, the laser from the interferometer reflected from the DM to the flip mirror, then back to the DM and into the interferometer, thus preventing the laser from reaching the CFRP mirror. This allowed for the collection of DM-only wavefront error data. Of note, the interferometer compensates for the double-pass induced by single reflections off a surface by dividing all measurements by 2. However, since the laser hits the DM twice in the “flip mirror UP” configuration, all DM-only wavefront error measurements required an additional division by 2 to compensate for the second reflection. With the flip mirror

DOWN, the full optical path was allowed. As seen in Figure 10, having the flip mirror in the DOWN position allowed the laser from the interferometer to reflect from the DM to the CFRP mirror, and then back to the DM and into the interferometer. Since the laser reflects off the CFRP mirror only once, the CFRP wavefront measurements did not require additional double-pass corrections.

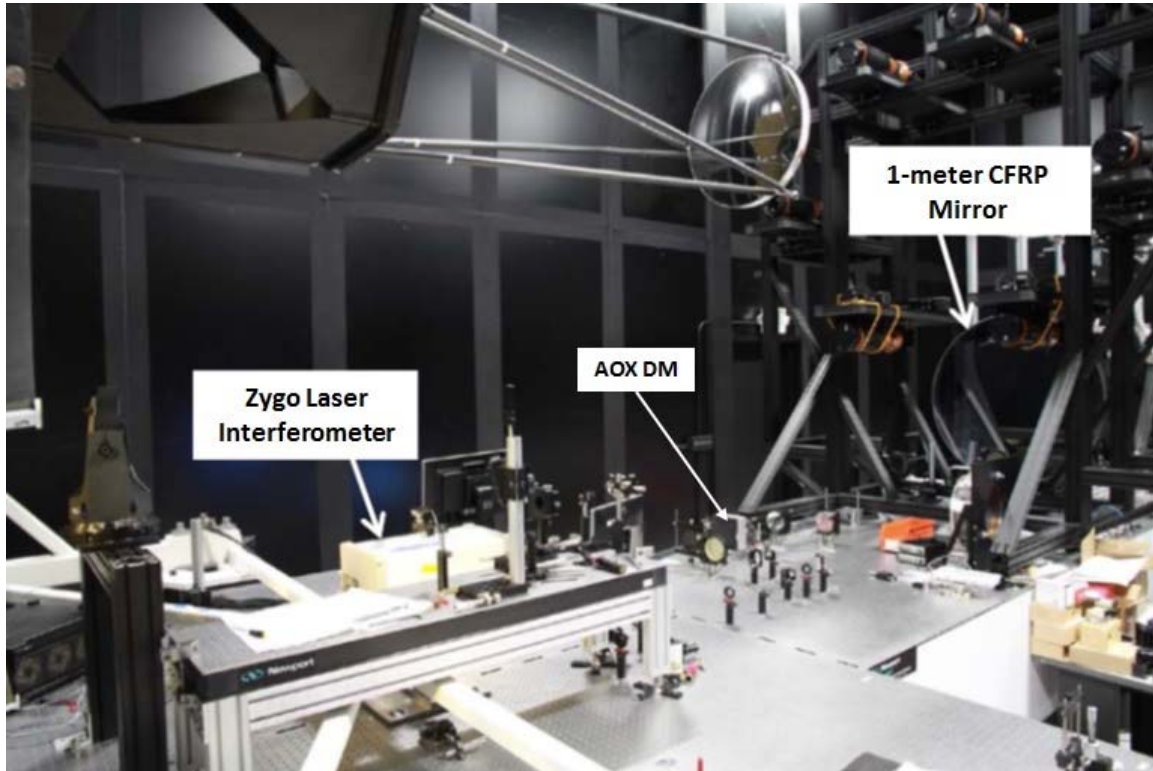


Figure 9. 1-meter CFRP Mirror Optical Layout

Adapted from [4]: J. J. Kim, M. Allen and B. Agrawal, “Cost-effective aperture with deformable mirror for imaging satellites,” presented at the 66th International Astronautical Conference, Jerusalem, Israel, 2015.

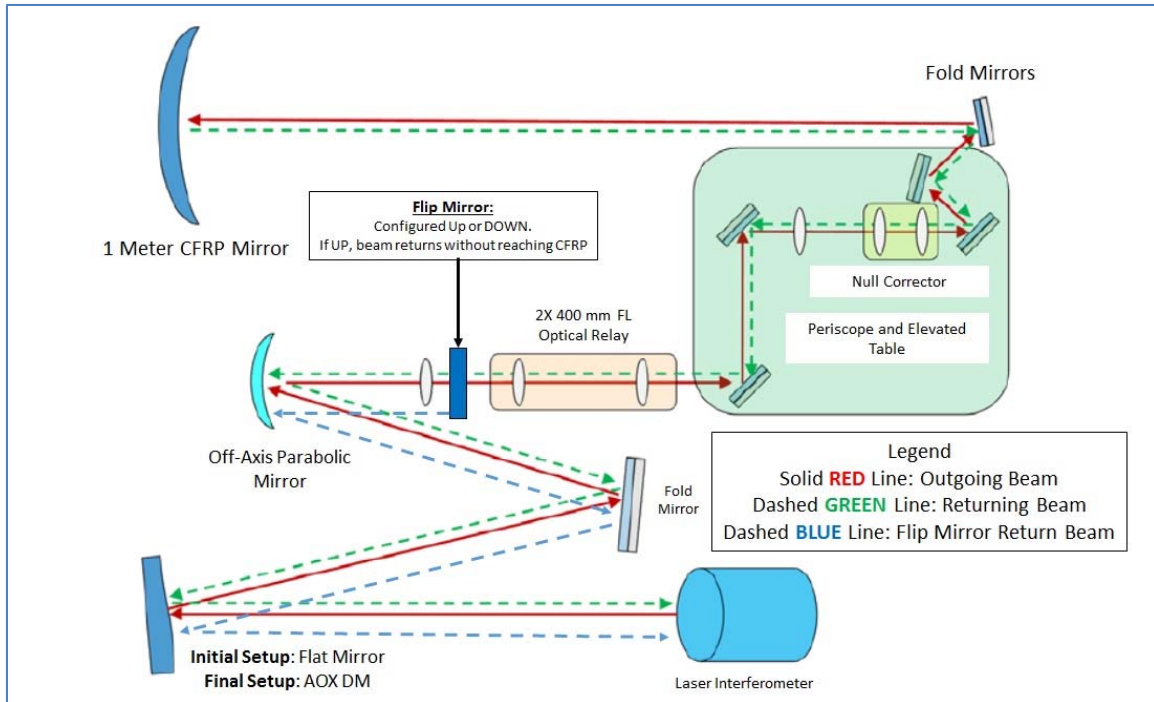


Figure 10. 1-meter CFRP Mirror Optical Layout Schematic

Adapted from [5]: B. N. Agrawal, Jae-Jun Kim and M. Allen, “Cost-effective large apertures for future imaging satellites,” presented at the *AIAA SPACE Conference*, Pasadena, CA, 2015, vol. 4494.

Figure 11 presents the workstation layout for the experiments, which included 3 PC’s (Control, Zygo and AOX DM) connected via a transmission control protocol/Internet protocol (TCP/IP) connection. This connection enabled the Control PC to communicate and command the AOX DM and Zygo PC’s. To run the experiments, 2 separate MATLAB scripts (one on the Control PC and the other on the AOX DM PC) were required. The MATLAB script on the Control PC commanded the MetroPro software on the Zygo PC to collect and return the wavefront sensor data to the Control PC for processing. The Control PC then generated and sent the required DM control commands to the AOX DM PC via a TCP/IP connection. The AOX DM PC was the primary interface with the DM. It ran a MATLAB script that received the inputs from the Control PC, then loaded those inputs into the DM via the WinHVA software. This process was repeated for each DM control iteration. A schematic of the experimental workstation presented in Figure 12.

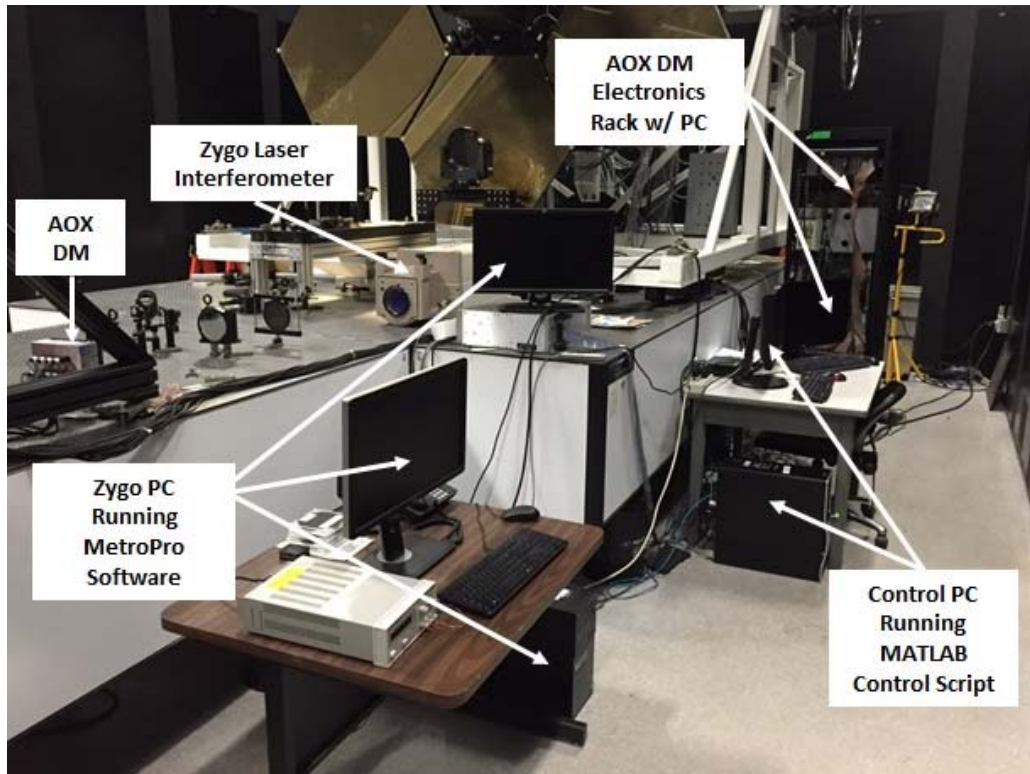


Figure 11. Experimental Workstation Layout

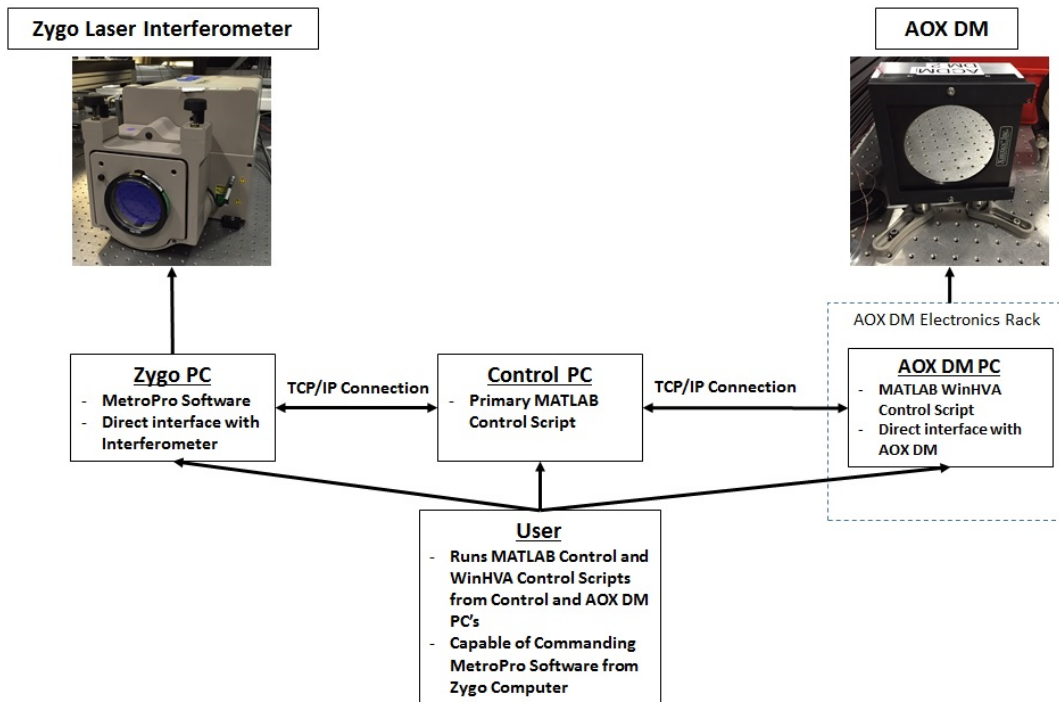


Figure 12. Experimental Workstation Schematic

B. CFRP MIRROR SURFACE ERROR CHARACTERIZATION

The surface of the CFRP mirror was characterized via interferometric wavefront measurements conducted with a flat mirror in the optical path. Figure 13 presents the measured wavefront error of the CFRP mirror with piston, tip and tip removed and no measurement mask applied. Piston, tip and tilt aberrations are a function of the relative position between the mirror and the interferometer, hence they are not an indicator of the surface figure error of the mirror. As discussed by Agrawal et al. in [5], the CFRP mirror at NPS suffers from several manufacturing defects. The principal defect is the failure of the mirror's center core, which occurred during the removal of the CFRP mirror from the mandrel [5]. This core structure failure is responsible for the large areas of data dropout present in the center section of the mirror. Figure 13 also shows wavefront data dropouts in the top-middle and top-left sections of CFRP mirror. These data dropouts are due to other manufacturing defects [5]. In addition, Figure 13 shows the hexagonal print-through of the mirror's core structure, which increases the mirror's total wavefront error [5]. The measured RMS and PV error values for the CFRP were 1.372 waves and 7.963 waves, respectively. In the work performed by Agrawal et al. in [5], the CFRP mirror at NPS was analyzed to determine the number of actuators required to correct the dominant spatial frequencies in the wavefront error. Via a 2-dimensional fast Fourier transform (2-D FFT), the CFRP mirror was determined to have dominant spatial frequencies as high as 75 cycles per aperture [5]. Since the number of required actuators is directly proportional to the spatial frequency of the wavefront error, a DM with a 75 by 75 grid of actuators (5625 total actuators) would be required to remove the dominant spatial frequencies from the CFRP mirror [5]. A DM of that size is not commercially available. However, a significant reduction in RMS wavefront error can be achieved with 400 actuators or less [5]. For this reason, the 349 actuator AOX DM currently at NPS was selected for this thesis work.

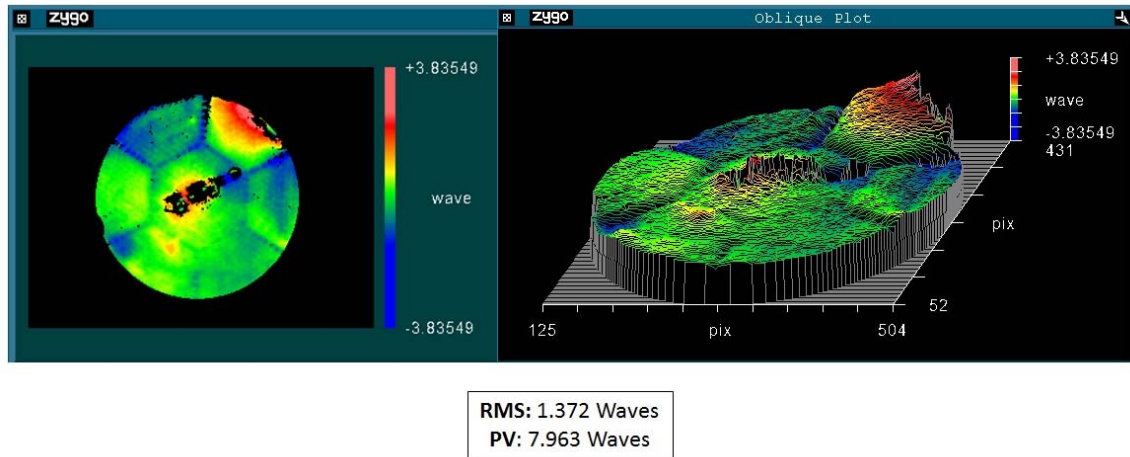


Figure 13. CFRP Baseline Error with No Masking

For the purposes of this thesis, the defective areas of the CFRP mirror were masked in order to depict future CFRP mirror quality. As CFRP manufacturing processes mature, the amount and severity of manufacturing defects is expected to decrease, thus leading to CFRP mirrors with improved surface quality. Masking the defective areas of the mirror also benefits the performance of the DM, since the actuators are less likely to saturate due to the reduced strength of the wavefront errors. For this thesis, it was decided to mask the defective center section and the upper two panels of the CFRP mirror. The decision to mask the upper two panels completely was based on the high number of inoperable DM actuators that corresponded to those areas. The baseline DM surface and the status of the DM actuators will be presented in the next section. Figure 14 shows the baseline CFRP wavefront error with the selected mask applied. Applying the mask reduced the measured RMS and PV error values to 0.351 waves and 2.691 waves, respectively. These RMS and PV error values will be utilized as the baseline CFRP wavefront error for this thesis. Table 3 presents a summary of the RMS and PV error values for the masked and unmasked CFRP measurements.

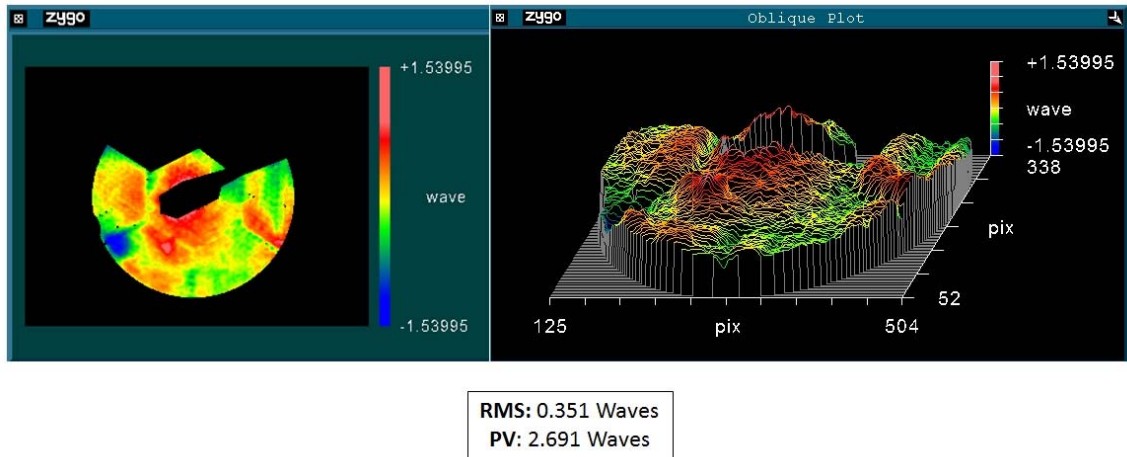


Figure 14. CFRP Baseline Error with Mask Applied

Table 3. Summary of CFRP RMS and PV Error Values

CFRP Mirror Parameter	Value (Waves)
RMS with Mask	0.351
PV Error with Mask	2.691
RMS without Mask	1.372
PV Error without Mask	7.963

C. DM BASELINE SURFACE

The surface of the AOX DM was characterized via interferometric wavefront measurements conducted with the CFRP optical layout in the “flip mirror UP” configuration. The AOX DM was powered but all actuators were commanded to the neutral 0 V position. This operational state will be referred throughout this thesis as the AOX DM baseline state. Figure 15 presents the measured baseline wavefront error of the AOX DM. As seen in Figure 15, the DM exhibits an RMS error of 0.294 and a PV error of 2.036. When the CFRP optical layout is in the “flip mirror DOWN” configuration, the baseline AOX DM wavefront error will be combined with the CFRP baseline error to yield the total wavefront error of the system.

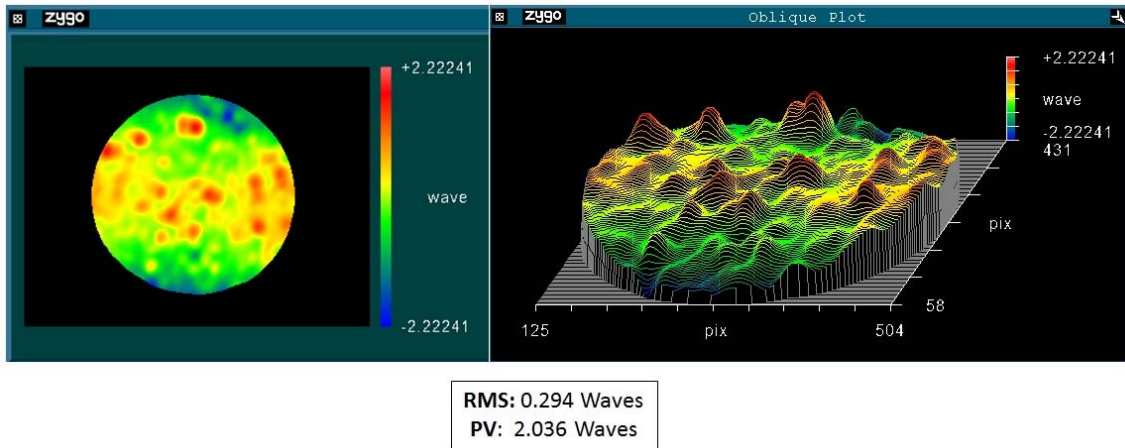


Figure 15. AOX DM Baseline Wavefront Error

During the surface characterization of the AOX DM, all actuators were checked for proper performance. This check consisted of applying positive and negative voltages to each actuator, and noting any discrepancies. In total, 7 actuators were determined to be inoperable and 10 actuators were determined to have marginal performance. The actuators with marginal performance were characterized by an unreliable response to actuator voltage commands. Figure 16 depicts the AOX DM actuator layout with inoperable and marginal actuators highlighted. In addition, two actuators were identified as being shorted together, hence a voltage application to either actuator resulted in a response from both actuators. As shown in Figure 16, the majority of the inoperable and marginal actuators were located in the upper section of the DM. Since the DM correction capability is limited in those areas, the decision was made to mask out the areas of the CFRP mirror that corresponded to the upper section of the DM. Figure 17 shows the baseline error for the DM with the CFRP masked applied. As expected, the resultant RMS and PV error values decreased to 0.277 and 1.957, respectively. Table 4 presents a summary of the RMS and PV error values for the masked and unmasked DM measurements.

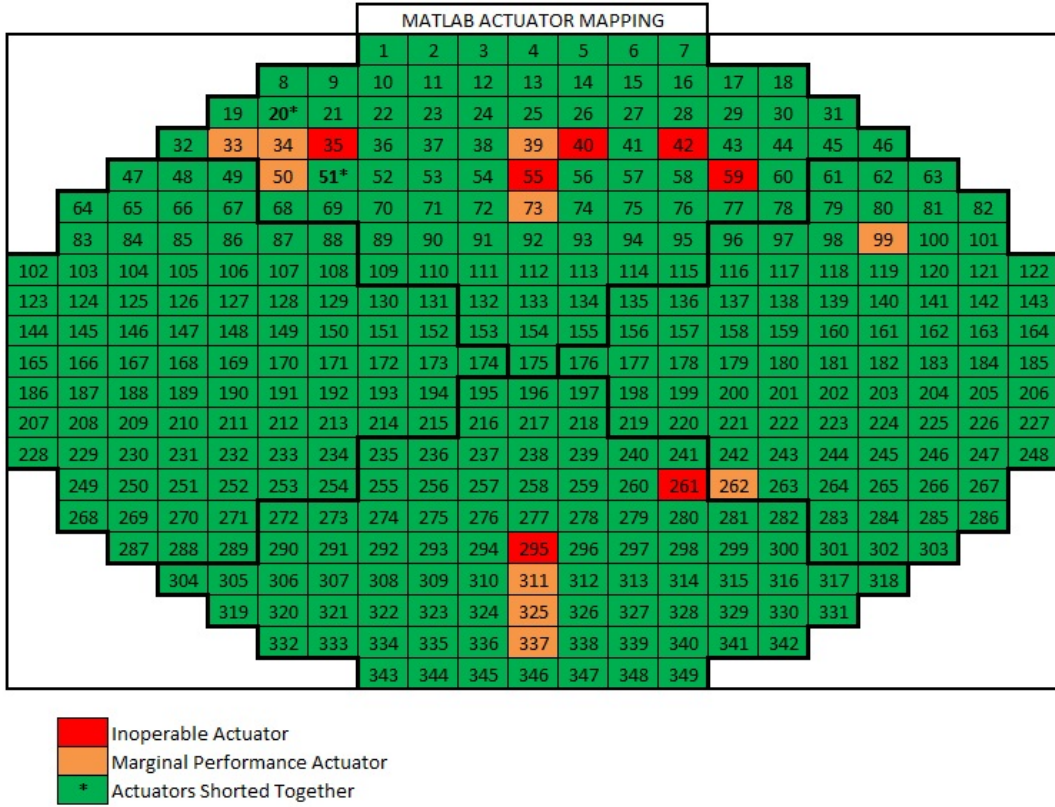


Figure 16. AOX DM Actuator Layout—Inoperable Actuators Highlighted

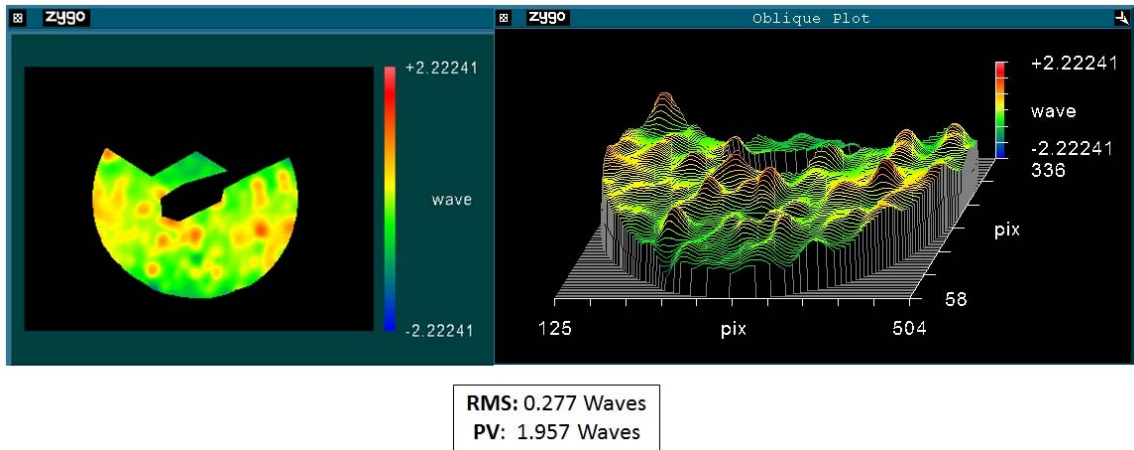


Figure 17. AOX DM Baseline Image with Mask Applied

Table 4. Summary of DM RMS and PV Error Values

DM Parameter	Value (Waves)
RMS without Mask	0.294
PV Error without Mask	2.036
RMS with Mask	0.277
PV Error with Mask	1.957

D. AO SYSTEM BASELINE ERROR

The baseline wavefront error of the AO system, which results from the combined effect of the surface errors present in both the CFRP Mirror and AOX DM, was characterized with the CFRP optical layout in the “flip mirror DOWN” configuration and with the measurement mask applied. The AOX DM was in the baseline state. The measurement results are presented in Figure 18. As expected, the combined RMS and PV error values are larger than the individual measurements taken of the CFRP mirror and AOX DM. Of note, the CFRP measurement data suffered from an increased number of data dropouts due to the noise created by the DM electronics fan assembly. As compared to the AOX DM, the CFRP mirror had an increased sensitivity to acoustic vibrations. This was due to its large parabolic shape and lightweight material properties. For this reason, the DM only measurements did not experience data dropouts due to the acoustic energy generated by the DM fan assembly. The DM utilized in this thesis was originally acquired by NPS for high energy laser AO applications, which are less sensitive to acoustic vibrations than large parabolic lightweight mirrors.

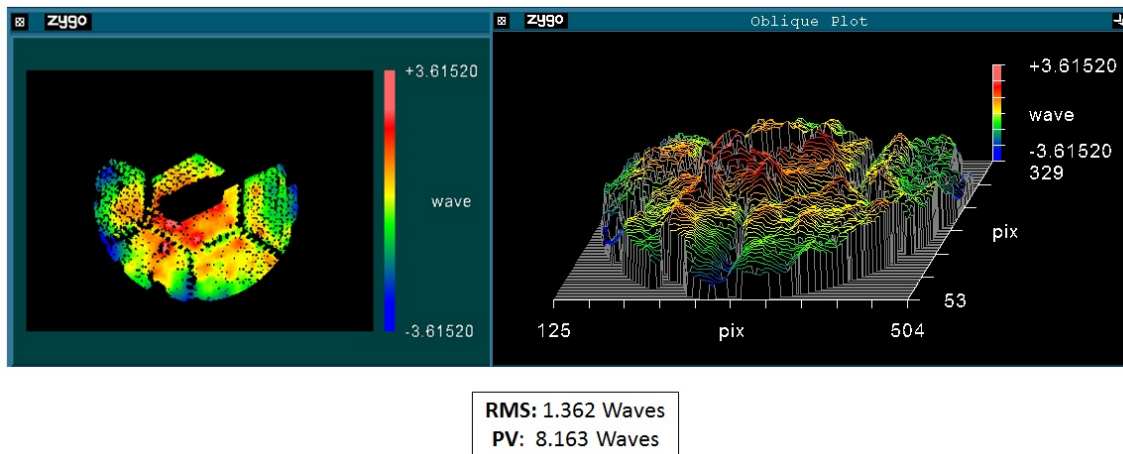


Figure 18. Typical Baseline AO System Wavefront Error

In summary, the AO system must have the capability to reduce the total system wavefront error from approximately 1.362 waves to below 0.351 waves, which is the CFRP baseline error. An AO system that does not meet this requirement will be considered ineffective.

THIS PAGE _INTENTIONALLY LEFT BLANK

IV. CONTROL METHOD

In this thesis, an integral control system was utilized to reduce the surface performance requirements the CFRP mirror at NPS. A schematic of the AO control system utilized in this thesis is presented in Figure 19.

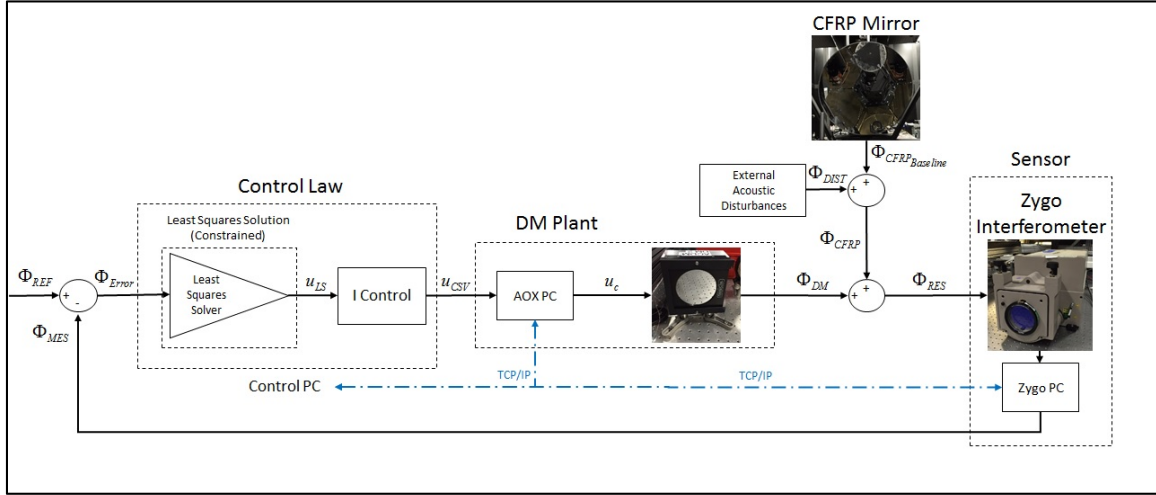


Figure 19. Schematic of Experimental AO Control System

The reference wavefront (Φ_{REF}) was a 120438 by 1 vector of zeros, since this corresponded to the desired error free wavefront. The size of the reference wavefront vector was dictated by the size of the interferometer measurement, which consisted of a 398 by 398 matrix that contained 120438 data points after processing (which consisted of data scaling and piston, tip and tilt removal). The reference wavefront was compared to an initial wavefront measurement (Φ_{MES}) to generate an initial wavefront error vector (Φ_{Error}). The control law was contained within a MATLAB script located in the Control PC. The control law consisted of calculating a least-squares control solution (u_{LS}) that was scaled by an integral control gain. The least-squares solution was calculated utilizing the Influence Matrix (Γ) of the DM and was implemented with a constraint on the maximum/minimum allowable DM voltage command [18]. Specific details on the least-squares solution and the development of the Influence Matrix (Γ) will be presented in

the next three sections. The output of the control law was a CSV file that contained the desired command voltages for the DM in counts from -2048 to 2047. This file was loaded into the WinHVA software by a MATLAB script located in the AOX DM PC. The WinHVA software was the direct connection to the DM hardware and generated a control signal (u_c) that contained the necessary commands to actuate the DM. The residual wavefront error (Φ_{RES}) was a combination of the resultant DM wavefront (Φ_{DM}) and CFRP wavefront errors (Φ_{CFRP}). The CFRP baseline wavefront error ($\Phi_{CFRP_{Baseline}}$) was augmented by external acoustic disturbances (Φ_{DIST}). The largest acoustic disturbance was due to the DM electronics rack, which housed three cooling fans that generated white noise. The fans were a critical element of the DM system, hence the DM could not be operated without the cooling fans. Operation without the cooling fans would have resulted in DM system failure. As mentioned in the previous chapter, the AOX DM was developed for a high energy laser AO application that was insensitive to the acoustic disturbances generated by the DM electronics rack. The residual wavefront error was then measured by the Zygo interferometer system, which generated a measured wavefront (Φ_{MES}) vector that was subtracted from the reference wavefront to generate an updated wavefront error vector. To mitigate the effects of the acoustic disturbance, the interferometer collected and averaged three separate measurements. In addition, piston, tip and tilt were removed from the averaged measurements since these optical aberrations were not a result of the surface figure error of the CFRP. This prevented premature DM actuator saturation. The feedback loop presented in Figure 19 continued until the updated wavefront vector reached a steady state value.

In addition to the experimental work performed in this thesis, control simulations were performed to establish a “best case” control scenario. A schematic of the simulation control system is presented in Figure 20. In the simulation control system, the DM wavefront was estimated by multiplying the Influence Matrix (Γ) by the control vector (u_c). The sensor measurement was simulated by adding the estimated DM wavefront to a combined DM and CFRP baseline measurement. The simulated control system was implemented via a MATLAB script.

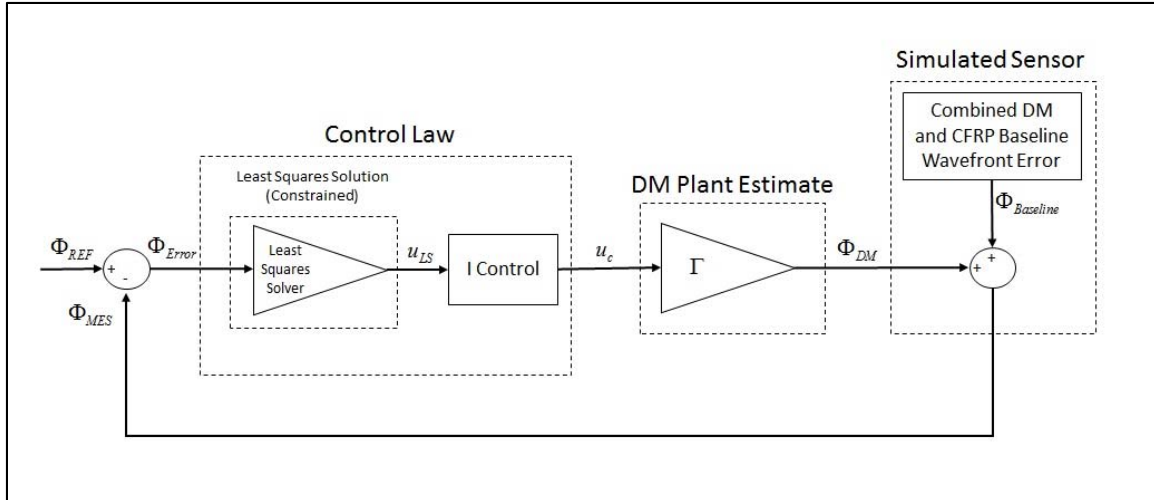


Figure 20. Schematic of Simulated AO Control System

A. INFLUENCE MATRIX COLLECTION

The influence matrix collection process for the DM started by gathering a baseline wavefront error measurement. The baseline measurement was collected with the DM in the baseline state (DM powered, all actuators set to 0 V). Next, the each actuator was commanded individually to an arbitrary value of 14.65 mV. After each actuator command, a wavefront measurement was collected. The DM baseline wavefront measurement, piston, tip and tilt were then subtracted from the single actuator wavefront measurement. This yielded the wavefront influence of the single actuator. Figure 21 shows the wavefront influence of actuator 70.

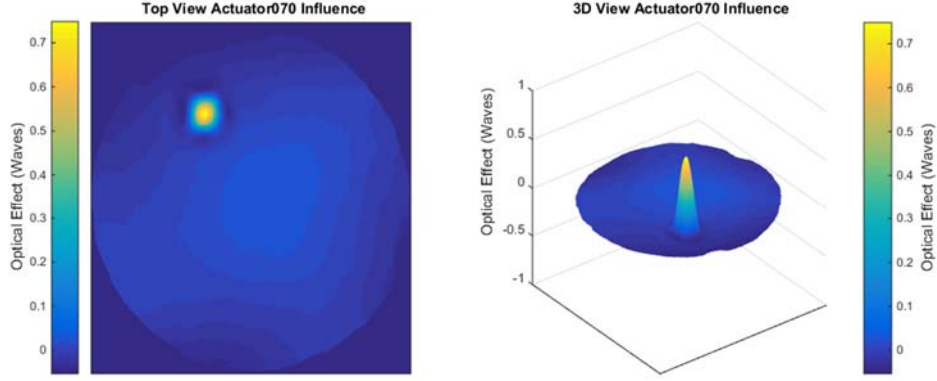


Figure 21. Wavefront Influence of Actuator 70

The collected single actuator wavefront influence was reshaped into a 120438 by 1 vector, then stored at its corresponding column in the influence matrix. Hence, the size of this initial influence matrix was 120438 by 349. Equation 4.1 shows the organization of the initial Influence Matrix (Γ_i).

$$\Gamma_i = \begin{pmatrix} \phi_{1,1} & \cdots & \phi_{1,349} \\ \vdots & \ddots & \vdots \\ \phi_{120438,1} & \cdots & \phi_{120438,349} \end{pmatrix} \quad (4.1)$$

The initial influence matrix in Equation 4.1 was analyzed to determine its condition number. The condition number of a matrix is defined as the ratio between the largest and smallest singular value. A “well-conditioned” matrix has a small condition number, while an “ill-conditioned” matrix has a high condition number. For example, the condition number of a singular matrix is infinity. If a matrix is ill-conditioned, calculating its inverse could be problematic and the results might be unreliable. The condition number of the influence matrix is important for least-squares problems since least-squares solutions require the inversion of the influence matrix. Equation 4.2 shows the condition number calculation for a generic matrix A.

$$cond[A] = \frac{\sigma_{Max}}{\sigma_{Min}} \quad (4.2)$$

In Equation 4.2, the terms σ_{Max} and σ_{Min} correspond to the maximum and minimum singular values, respectively. The MATLAB command “cond(A)” was utilized for this calculation. The condition number for the initial influence matrix in Equation 4.1 was 580.7. To visualize the singular values of the influence matrix, a reduced singular value decomposition (SVD) was performed on the influence matrix. The reduced SVD for a generic matrix A is presented in Equation 4.3.

$$A = \hat{U} \hat{\Sigma} V^* \quad (4.3)$$

The SVD is a type of modal decomposition technique that yields the singular values and the SVD modes of the generic matrix A. In Equation 4.3, a generic matrix A is decomposed into three separate matrices. The $\hat{\Sigma}$ matrix is a diagonal matrix that contains the singular values. The MATLAB command “[U, S, V] = svd(A,0)” was utilized for this calculation. The normalized singular values of the influence matrix are plotted in Figure 22. From Figure 22, it is evident that there is a large disparity between the highest and lowest singular values.

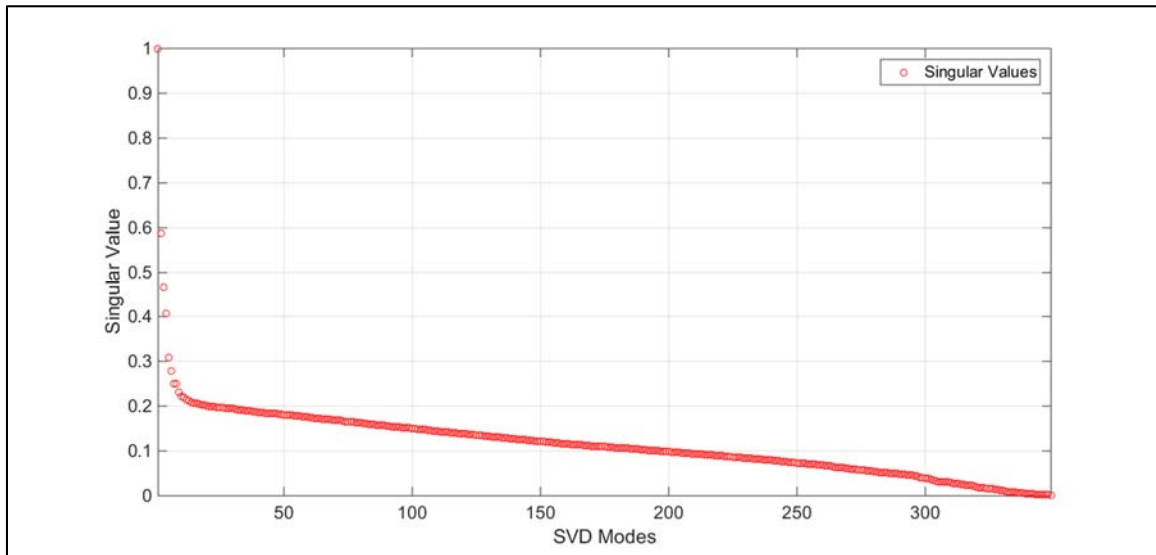


Figure 22. Singular Values of the Initial Influence Matrix

The difference between the maximum and minimum singular values was reduced by removing from the influence matrix any actuators that had an insignificant influence

on the wavefront. The insignificant actuators were identified by plotting and evaluating the wavefront influence of each actuator. This analysis identified that some of the edge actuators did not have significant influence on the wavefront. In addition, the analysis confirmed that the previously identified inoperable actuators did not have an influence on the wavefront. Based on this analysis, a total of 38 edge and 7 inoperable actuators were removed from the influence matrix. The removal of the edge and inoperable actuators reduced the size of the influence matrix to 120438 by 304, and reduced the condition number from 580.7 to 40.4. The singular values of the reduced influence matrix are presented in Figure 23.

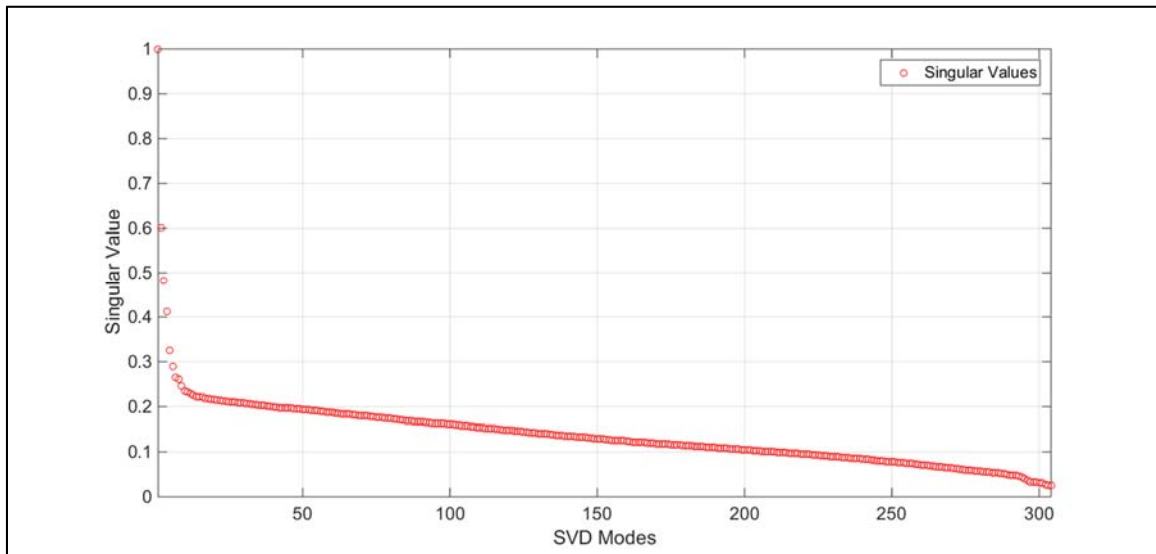


Figure 23. Singular Values of the Reduced Influence Matrix

The marginal performance actuators identified in Chapter III were not removed from the influence matrix since their influence could still be significant. Equation 4.4 shows the reduced influence matrix, which will be referred to as the Influence Matrix (Γ) for the remainder of this thesis. Figure 24 highlights the removed actuators. The marginal performance actuators are also presented in Figure 24 for reference. As will be discussed in the next section, the Influence Matrix (Γ) was utilized to generate the least-squares control solution.

$$\Gamma = \begin{pmatrix} \phi_{1,1} & \cdots & \phi_{1,304} \\ \vdots & \ddots & \vdots \\ \phi_{120438,1} & \cdots & \phi_{120438,304} \end{pmatrix} \quad (4.4)$$

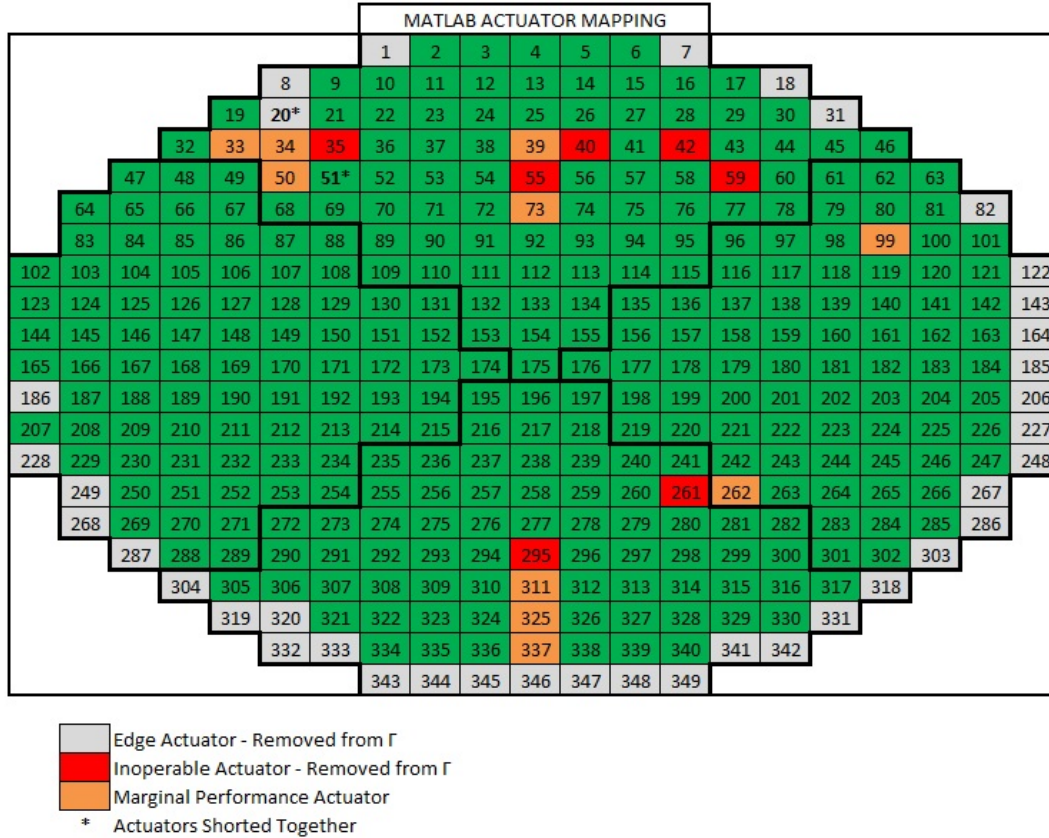


Figure 24. AOX DM Actuator Evaluation

B. LINEAR LEAST-SQUARES CONTROL

The influence matrix of the DM describes the optical influence each DM actuator [18]. Hence, it can be utilized to generate an estimate of the cumulative optical effect of the DM. For this estimate to be accurate, two assumptions are required. First, the columns of the influence matrix must be linearly independent. Second, the relationship between the actuator input voltage and the actuator optical effect must be linear. The first assumption was verified by calculating the rank of the influence matrix, which is the number of non-zero singular values and presents the number of linearly independent

columns. It can be seen from Figure 23 that all the singular values of the influence matrix are non-zero. The second assumption was verified by the AOX DM documentation, which states that the operating voltage range of the electronics rack (-70 V to 40 V) is within the linear range of the actuators [12]. An estimate of the cumulative optical effect of the DM can be calculated via Equation 4.5.

$$\Gamma u = \Phi_{DM} \quad (4.5)$$

In Equation 4.5, u is the DM control vector and Φ_{DM} is the estimated optical effect of the DM. All AO systems are based on the principle of phase conjugation, which states that a DM must deform the shape of its reflective surface to match the inverse of the incoming wavefront error shape [6]. Hence, to arrive at the desired control solution (u), the system must minimize the residual value presented in Equation 4.6. To conform to the phase conjugation principle, the control input to the DM will be the negative of the control value depicted in Equation 4.6.

$$r = \Gamma u - \Phi_{MES} \quad (4.6)$$

In Equation 4.6, Φ_{MES} represents the residual wavefront error vector as measured by the interferometer. Since Equation 4.6 is an overdetermined system (Γ has more rows than columns), the residual value (r) in Equation 4.6 cannot be reduced to zero. Hence, a mathematical method to minimizing the residual value (r) is required. One method to minimize the residual (r) is the linear least-squares approximation [19], [20]. This method calculates a control value (u) that approximates the solution to Equation 4.7 by minimizing the least-squares residual value in Equation 4.8 [19], [20].

$$\Gamma u = \Phi_{MES} \quad (4.7)$$

$$\text{Find } u \text{ that minimizes: } r_{LS} = \frac{1}{2} \left\| \Gamma u - \Phi_{MES} \right\|_2^2 = \frac{1}{2} \left\| r \right\|_2^2 \quad (4.8)$$

Equation 4.8 calculates the square of the 2-norm of the residual value presented in Equation 4.6. As presented in Equation 4.9, a solution to the linear least-squares problem presented in Equations 4.7 and 4.8 can be calculated by computing the pseudoinverse of

the Influence Matrix (Γ^\dagger) and multiplying it by the measured residual wavefront error vector (Φ_{MES}).

$$u = (\Gamma^T \Gamma)^{-1} \Gamma^T \Phi_{MES} = \Gamma^\dagger \Phi_{MES} \quad (4.9)$$

The calculation presented in Equation 4.9 is considered to be unconstrained since it does not take into account the current voltage state of the DM actuators or the maximum allowable DM control voltage. Due to the high acoustic noise experienced by CFRP mirror as a result of the DM electronics rack, the unconstrained control approach presented in Equations 4.7 through 4.9 will result in premature actuator voltage saturation. To prevent this, the linear least-squares solution was modified to include maximum and minimum bounds on the control voltage. The constrained linear least-squares algorithm presented in this section was based on the thesis work performed by Watson [18]. The constrained linear least-squares solution will consist of solving the problem outlined in Equation 4.10 [18].

$$\begin{aligned} \text{Find } u \text{ that minimizes: } & \frac{1}{2} \|\Gamma u - \Phi_{MES}\|_2^2 \\ \text{subject to } & lb \leq u \leq ub \end{aligned} \quad (4.10)$$

In Equation 4.10, lb and ub refer to the lower and upper bounds of the available actuator control voltage, respectively. The lower and upper bound control voltage values were calculated for each control iteration. This control scheme took into account the available performance of each actuator when calculating actuator commands [18], thus limiting premature actuator saturation due to the acoustic noise. Equations 4.11 and 4.12 present the lower and upper bound calculations.

$$u_{lb} = u_{\min_{304 \times 1}} - u_{\text{Prev}_{304 \times 1}} = \begin{pmatrix} -30V \\ \vdots \\ -30V \end{pmatrix} - \begin{pmatrix} u_{\text{Prev}1} \\ \vdots \\ u_{\text{Prev}304} \end{pmatrix} \quad (4.11)$$

$$u_{ub} = u_{\max_{304 \times 1}} - u_{\text{Prev}_{304 \times 1}} = \begin{pmatrix} 30V \\ \vdots \\ 30V \end{pmatrix} - \begin{pmatrix} u_{\text{Prev}1} \\ \vdots \\ u_{\text{Prev}304} \end{pmatrix} \quad (4.12)$$

The constrained least-squares solution was implemented via the LSQLIN function in MATLAB [18], [20]. The inputs to the LSQLIN function were the DM influence matrix, the current sensor measurement, the upper and lower bounds for the control, and the previous control command (initial condition for the function). A sample MATLAB command to generate a control command (u) utilizing LSQLIN is presented in Equation 4.13.

$$u_{LS} = \text{LSQLIN}(\text{InfluenceMatrix}, \text{WavefrontErrorVector}, [], [], [], [], u_{lb}, u_{ub}, u_{initial}) \quad (4.13)$$

In Equation 4.13, the blank entries in LSQLIN correspond to unused functions such as equality constraints, which were not applicable for this thesis.

C. CONTROL SCRIPT IMPLEMENTATION

The integral control system depicted in Figure 19 was implemented via a MATLAB script that executed an iterative control loop. In the script, the integral controller is achieved by calculating a scaled intermediate control solution (u_{Delta}) and adding it to the previous control solution (u_{Prev}). This generated an updated control solution (u_{Next}) for the AO system, as depicted in Equation 4.14. The initial control vector for all simulations and experiments was an all zero vector, since this corresponded to the baseline state of the DM. The iterative control process was repeated until the controller converged on a solution.

$$u_{Next} = u_{Prev} + u_{Delta} \quad (4.14)$$

To generate u_{Delta} , a wavefront error signal (Φ_{Error}) was calculated by subtracting the measured residual wavefront error vector (Φ_{MES}) from a reference wavefront error vector (Φ_{REF}) of all zeros. This is depicted in Equation 4.15.

$$\Phi_{Error} = \Phi_{REF} - \Phi_{MES} = -\Phi_{MES} \quad (4.15)$$

The wavefront error signal (Φ_{Error}) was then utilized to generate a constrained linear least-squares solution utilizing the MATLAB function LSQLIN presented in Equation 4.13. This control solution was scaled by an integral control gain (K_i) and by a

voltage reference value (v_{REF}). A voltage reference value was required since the least-squares control solution was normalized by 14.65 mV (actuator control voltage utilized to generate the influence matrix). The integral control gain scaled the overall magnitude of the intermediate control solution, and determined the number of iterations required to converge on a solution. The calculation of the intermediate control solution is presented in Equation 4.16.

$$u_{Delta} = K_i (u_{LS} v_{REF}) \quad (4.16)$$

THIS PAGE INTENTIONALLY LEFT BLANK

V. CFRP MIRROR SURFACE ERROR CORRECTION

In this chapter, the results from both simulated and experimental CFRP mirror surface error corrections will be presented. The results from the simulations were used to establish how well the AO system should perform in an ideal environment. The simulated results represented a best case performance scenario for the AO system since the control simulations did not include outside disturbances or sensor measurement errors. The experimental work was performed to validate the concept of utilizing a DM to reduce the surface performance requirements of a CFRP primary mirror. The control technique discussed in the previous chapter was utilized to generate both simulated and experimental results. These results are presented in the next two sections.

A. SIMULATED CFRP MIRROR CORRECTION

A simulation of the AO control system was utilized to predict the performance of the control algorithm discussed in the previous chapter. In this simulation, there were no additional disturbances or noise injected into the system since the purpose of the simulation was to generate a best case scenario for the control system. In addition, the correlation between actuator performance and the influence matrix was perfect since the influence matrix was utilized to estimate the DM optical effect (vice an interferometer). In the actual AO system, there will be some disparity between actual actuator performance and the influence matrix. A representative baseline wavefront error measurement was utilized for the simulation. This baseline measurement was gathered on 16 October 2015, and shows a typical CFRP interferometer wavefront measurement (with DM fan acoustic disturbance and measurement mask applied). The simulation consisted of iteratively applying the control law presented in the previous chapter until the corrected wavefront measurement achieved a steady state RMS value. The simulation results are presented in Figure 25. With an integral control gain (K_i) of 0.1, the simulated AO control system required 40 iterations to achieve a steady state RMS value of 0.208 waves. As seen in Figure 25, most of the actuator control voltages remained within $\pm 5V$, with a few actuators at approximately $\pm 15V$. This simulation demonstrated

that the DM could reduce the RMS of the CFRP mirror to approximately 0.208 waves in an environment with no additional disturbances and/or sensor noise. Of note, it is expected that the real actuator voltages will be much higher due to the DM fan acoustic disturbance present in the system (which affects the accuracy of the interferometer measurement for each iteration) and the imperfect correlation between the actuators and the influence matrix. A summary of the simulation results is presented in Table 5. These results highlight that the DM’s capability to reduce the CFRP RMS wavefront errors to levels below 0.351 waves. However, the simulated DM did not reduce the PV error below the CFRP Mirror Baseline Value. This is explained by the fact that the linear least-squares solution effectively minimizes the RMS of the wavefront error by minimizing the residual in Equation 4.8. This minimization does not take into account the maximum and minimum values of the wavefront error. Hence, the reduction in PV error is a byproduct of the minimization of the RMS error, but it is not a driving factor in the control law.

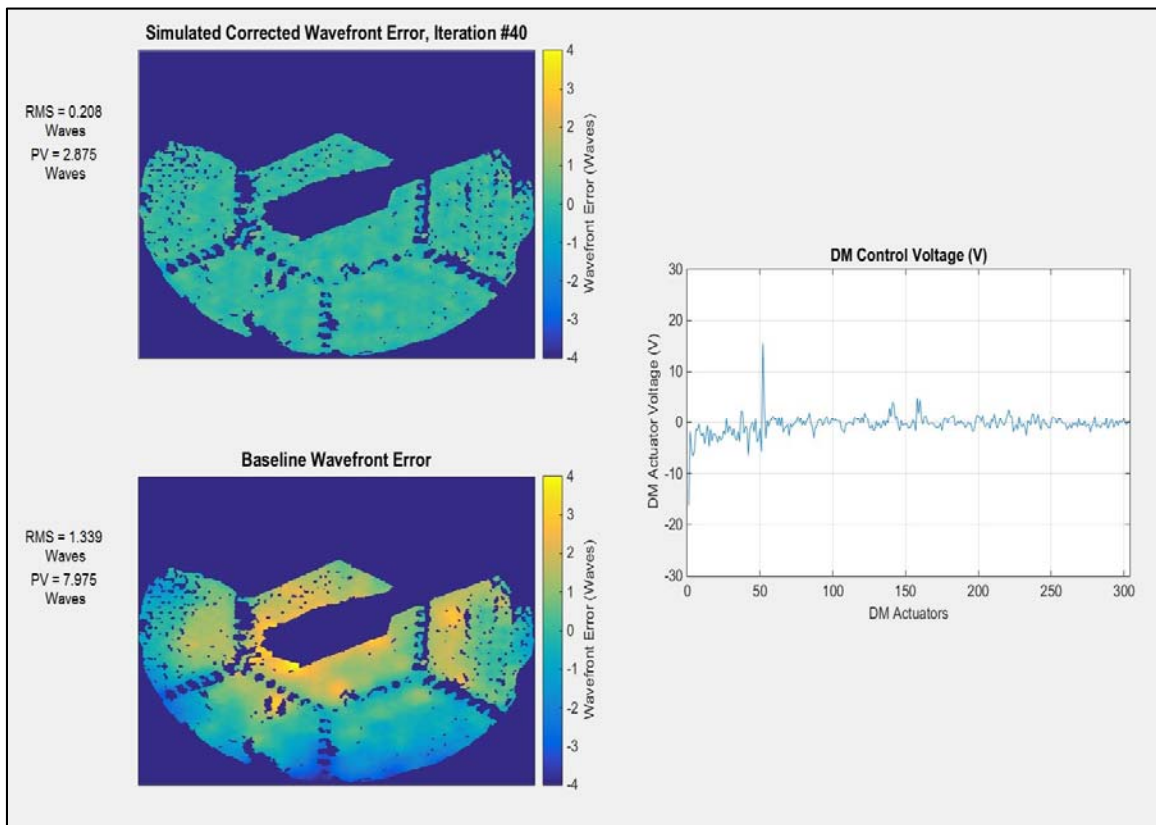


Figure 25. CFRP Error Correction Simulation Results

Table 5. Summary of CFRP Error Correction Simulation Results

Wavefront Measurement	RMS Error (Waves)	PV Error (Waves)
System Baseline Wavefront	1.339	7.975
CFRP Baseline Wavefront	0.351	2.691
Corrected Wavefront (Simulated)	0.208	2.875

B. EXPERIMENTAL CFRP MIRROR CORRECTION

In this section, experimental work validated the simulated results shown in Figure 25 and Table 5. As in the simulations, the integral control gain (K_i) was set to 0.1. The results of the experimental CFRP mirror wavefront error corrections are presented in Figure 26 and 27. Of note, the value of the baseline wavefront measurements varied based on room thermal conditions and outside disturbances. As a result, no two baseline wavefront error measurements were identical. As compared to the simulated results, the experimental results yielded higher residual RMS values (Figure 26) and higher control voltages (Figure 27). As mentioned in the previous section, this behavior was expected due to the presence of outside disturbances and the imperfect correlation between the DM actuators and the influence matrix. The actual AO control system required 46 iterations to achieve a steady state RMS value of 0.268 waves, vice the 40 iterations required by the simulation to achieve an RMS of 0.208 waves. Nevertheless, the experimental performance of the system yielded a 24% improvement in CFRP RMS error (as compared to the baseline CFRP RMS value of 0.351 waves), thus reducing the surface performance requirements of the mirror by 24%. From Figure 26 it can be seen that there are some areas in the CFRP mirror that did not correct well. These areas are highlighted in Figure 28.

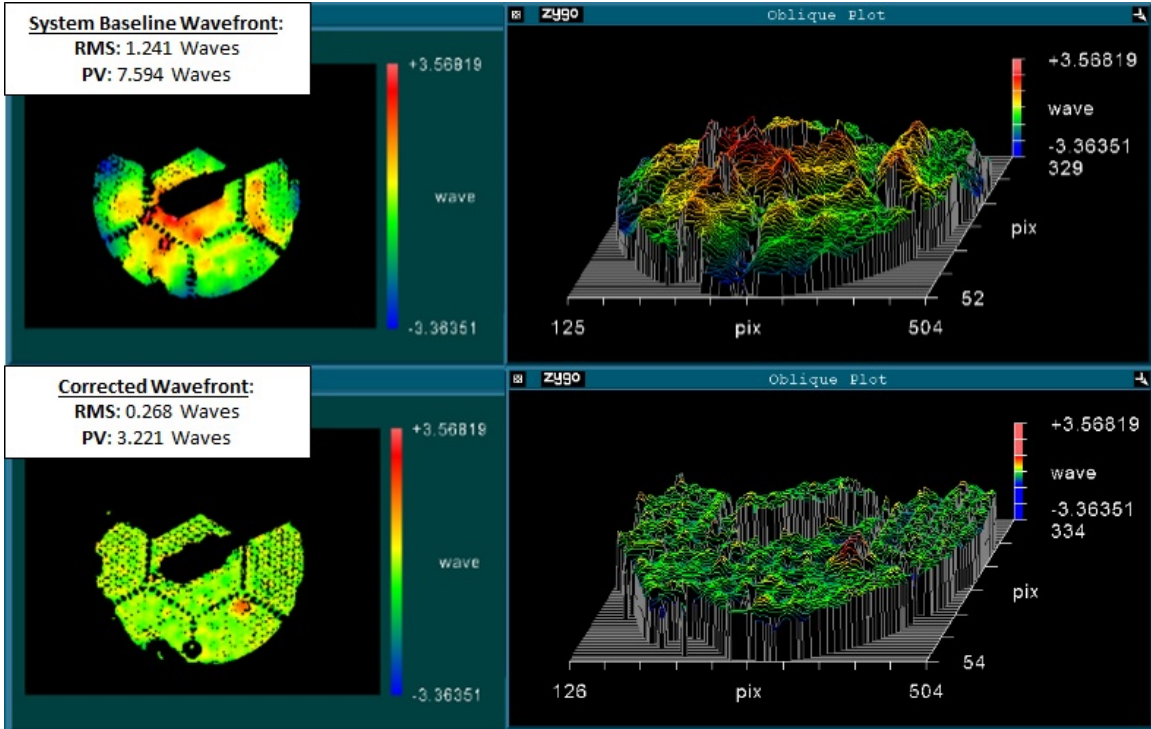


Figure 26. CFRP Error Correction Experimental Results

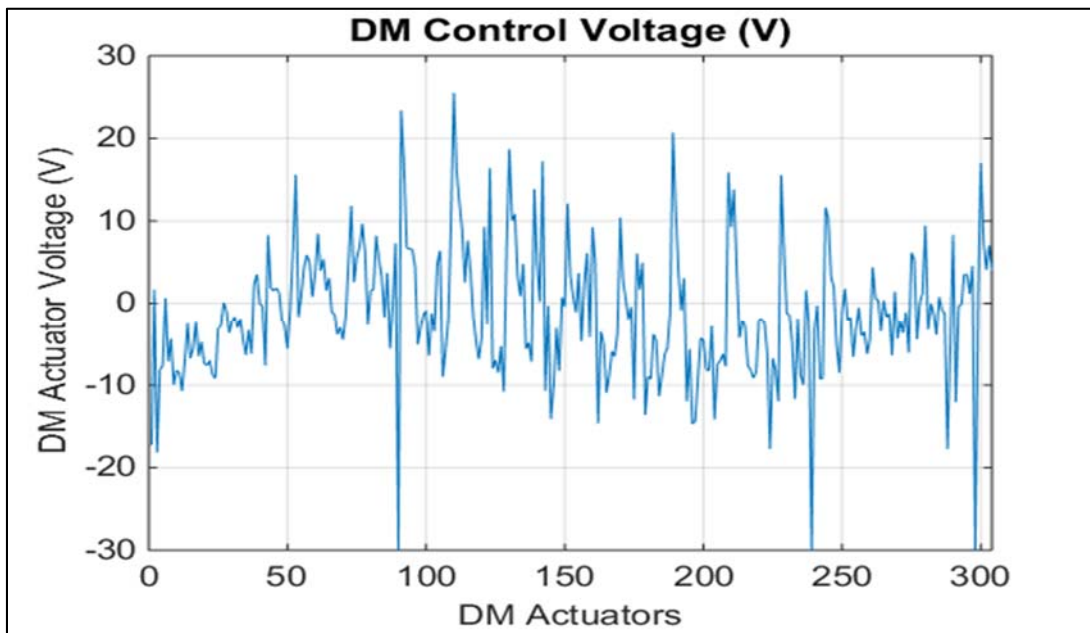


Figure 27. DM Control Voltage for Experimental CFRP Correction

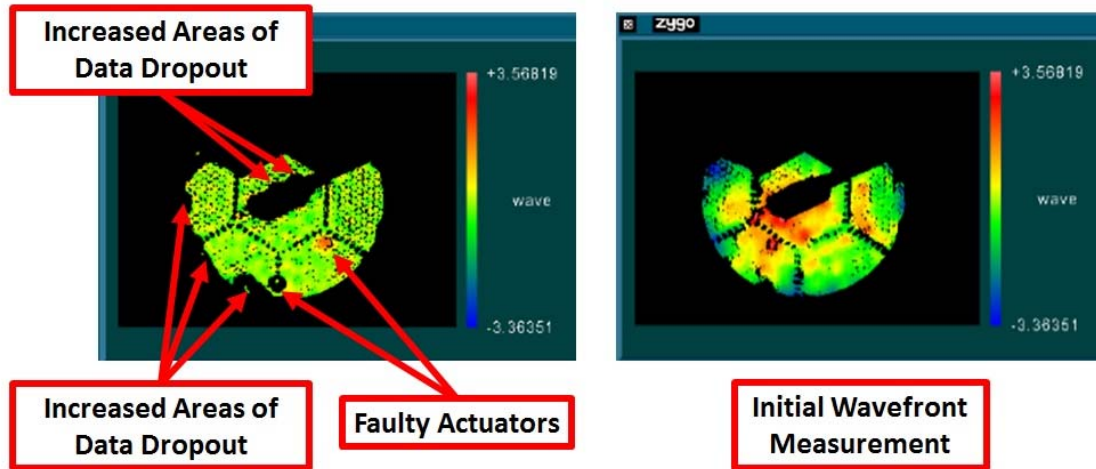
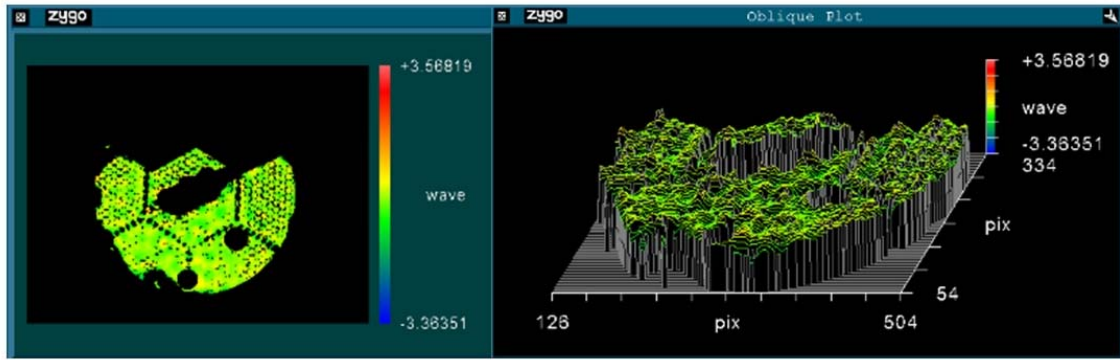


Figure 28. Data Dropout Comparison

As identified in Chapter 3, the combined system wavefront suffered from aberrations and data dropout areas as a result of CFRP mirror defects and DM fan acoustic disturbances. As seen in Figure 28, the DM corrected poorly around the edges of some areas with significant data dropout. This effect is most likely due to the measurement discontinuities caused by large areas of data dropouts, which are set to zero in the control law. Since the data dropouts are directly related to either CFRP manufacturing defects or DM fan acoustic disturbances, an AO control system without these inputs would not exhibit the behavior seen in Figure 28. In addition, Figure 28 highlights the sections uncorrected by faulty actuators. A further reduction of CFRP wavefront RMS error can be achieved by masking the 2 faulty actuators. These results are presented in Figure 29. With both faulty actuators masked, the residual RMS error reduces to 0.219 waves. This corresponds to a 38% improvement in CFRP RMS error (as compared to the baseline CFRP RMS value of 0.351 waves), thus reducing the surface performance requirements of the mirror by 38%. Table 6 summarizes the experimental results presented in this section.



RMS: 0.219 Waves
 PV: 2.42 Waves

Figure 29. CFRP Error Correction with Faulty Actuators Masked

Table 6. Summary of CFRP Error Correction Experimental Results

Wavefront Measurement	RMS Error (Waves)	PV Error (Waves)
System Baseline Wavefront	1.241	7.594
CFRP Baseline Wavefront	0.351	2.691
Corrected Wavefront	0.219	2.415
Improvement Over CFRP Baseline	RMS: 38%	PV: 10%

VI. CONCLUSION AND FUTURE WORK

A. REDUCTION IN CFRP SURFACE PERFORMANCE REQUIREMENTS

The research presented in this thesis experimentally validated the approach of utilizing DM to reduce the surface performance requirements of a CFRP mirror. The presented control technique yielded a 38 % reduction in CFRP RMS surface performance requirements. The reduction of CFRP RMS surface performance requirements is a critical step toward employing CFRP mirrors in future imaging satellites. The use of CFRP mirrors for space applications could yield substantial cost savings and could enable the development of large aperture imaging satellites.

B. FUTURE WORK

1. CFRP Mirror Suitability for the Space Environment

The physical characteristics of CFRP mirrors will need to be thoroughly evaluated for suitability with the space environment. Specifically, thermal and radiation effects should be evaluated for Low Earth Orbit (LEO), Medium Earth Orbit (MEO) and High Elliptical Orbit (HEO) and Geostationary Orbit (GEO) environments [21].

2. Imaging Satellite AO System Implementation

The experimental work performed in this thesis was conducted in a laboratory environment without consideration for the physical implementation of the AO system in an imaging satellite. The implementation of an AO system in an imaging satellite will be challenging since mass, power and volume are limited quantities in spacecraft. The location of the DM and wavefront sensors within the satellite's optical path, as well the overall mass and power of the system should be carefully considered. As another step toward future employment of CFRP mirrors in imaging satellites, a system study on AO satellite implementation should be developed [21].

THIS PAGE INTENTIONALLY LEFT BLANK

APPENDIX: MATLAB CODE

A. CFRP ERROR CORRECTION SIMULATION MATLAB CODE

```
% Post Final Results Simulation
clear
clc
% Load required data files
load Index_9Oct
load Mask_9Oct
load goodIFlist_30Oct_2
load index_GoodIF_30Oct_Fix_2
load IM_9OctGCH
load IM_9OctGCH_INV
load indexDM
load DMMask

% Baseline Measurement, 398x398, no PTT
% load('Baseline13-Oct-2015_2200.mat')
% load('Baseline22-Oct-2015_2106.mat')
load('Baseline16-Oct-2015_2107.mat') % Contains baselineDisp
file
Index_measurement = find(isnan(baselineDisp));
Mask_measurement = ones(398,398);
Mask_measurement(Index_measurement) = 0;

phase = baselineDisp;
phase(isnan(phase)) = 0; % set NaNs to zero
phaseVec = phase(Index_9Oct);
index = find(phase ~= 0);
phaseVecRMS = phase(index);
BaselineRMS = rms(phaseVecRMS);
RMS = rms(phaseVecRMS);
PV = max(phase(:)) - min(phase(:));
PV2 = PV;

% Control Loop:
m = 100; % Number of control
iterations
u = zeros(length(goodIFlist_30Oct_2),m);
uCount = zeros(length(goodIFlist_30Oct_2),m);
uCountMatrix = zeros(21,21);
uCountMatrixRec = zeros(21,21,m);
Gain = 0.05;
% Calculate voltage range of IM measurements
count = 800;
Volt_perCount = 14.65/1000; % V
VoltageRef = count*Volt_perCount;
phaseRes = zeros(length(Index_9Oct),m);
phaseRes(:,1) = phaseVec;

figure(1)
```

```

subplot(2,2,1), imagesc(baselineDisp), colorbar, caxis([-4 4])
c = colorbar;
c.Label.String = 'Wavefront Error (Waves)';
set(gca,'fontsize',16)
set(gca,'XTick',[]);
set(gca,'YTick',[]);
titleString = sprintf('Simulated Corrected Wavefront Error, Iteration
#%01d',i);
title(titleString), zlabel('Optical Effect (Waves)')
mTextBox = uicontrol('style','text');
RMSstring = sprintf('RMS = %1.3f Waves',RMS);
set(mTextBox,'String',RMSstring)
mTextBoxPosition = get(mTextBox,'Position');
set(mTextBox,'Position',[80 850 130 70])
set(mTextBox,'FontSize',14)
mTextBox2 = uicontrol('style','text');
PVstring = sprintf('PV = %1.3f Waves',PV);
set(mTextBox2,'String',PVstring)
mTextBoxPosition2 = get(mTextBox2,'Position');
set(mTextBox2,'Position',[80 800 130 70])
set(mTextBox2,'FontSize',14)
subplot(2,2,2), plot(u(:,1)), grid, xlabel('DM
Actuators','FontSize',14), set(gca,'FontSize',14)
ylabel('DM Actuator Voltage (V)','FontSize',14)
title('DM Control Voltage (V)','FontSize',16)
axis([0 304 -30 30])
subplot(2,2,3), imagesc(baselineDisp), colorbar, caxis([-4 4])
c = colorbar;
c.Label.String = 'Wavefront Error (Waves)';
set(gca,'fontsize',16)
set(gca,'XTick',[]);
set(gca,'YTick',[]);
title('Baseline Wavefront Error')
BaselineRMSstring = sprintf('RMS = %1.3f Waves',BaselineRMS);
pTextBox = uicontrol('style','text');
set(pTextBox,'String',BaselineRMSstring)
pTextBoxPosition = get(pTextBox,'Position');
set(pTextBox,'Position',[80 350 130 70])
set(pTextBox,'FontSize',14)
PVstring2 = sprintf('PV = %1.3f Waves',PV2);
pTextBox2 = uicontrol('style','text');
PVstring2 = sprintf('PV = %1.3f Waves',PV2);
set(pTextBox2,'String',PVstring2)
pTextBoxPosition2 = get(pTextBox2,'Position');
set(pTextBox2,'Position',[80 300 130 70])
set(pTextBox2,'FontSize',14)
pause()

% Optimization Parameters:
u_max = (30*ones(304,1))/VoltageRef; % scaled units
u_min = (-30*ones(304,1))/VoltageRef; % scaled units
u_ub = zeros(304,1);
u_lb = zeros(304,1);
for i = 1 : m
    u_prev = (u(:,i))/VoltageRef); % scaled units

```

```

u_ub = u_max - u_prev; % scaled units
u_lb = u_min - u_prev; % scaled units
u_opt =
lsqlin(IM_9OctGCH,phaseRes(:,i),[],[],[],[],u_lb,u_ub,u_prev); % scaled
units
u_delta = -Gain*(u_opt.*VoltageRef); % in Volts
%u_delta = Gain*((IM_9OctGCH_INV*phaseRes(:,i)).*VoltageRef);
u(:,i+1) = u(:,i) + u_delta; % in Volts
u_check = u(:,i+1);
u_check(u_check > 30) = 30;
u_check(u_check < -30) = -30;
u(:,i+1) = u_check;

% "Gather sensor data"
phaseRes(:,i+1) = IM_9OctGCH*u(:,i+1) + phaseVec;
phase(Index_9Oct) = phaseRes(:,i+1);
phase = phase.*Mask_measurement;
phaseVec2 = phase(Index_9Oct);
phaseRes(:,i+1) = phaseVec2;
phaseVecRMS = phase(index);
RMS = rms(phaseVecRMS);
PV = max(phase(:)) - min(phase(:));
phaseDisp = phase;
phaseDisp(phaseDisp == 0) = NaN;

% Display results:
subplot(2,2,1), imagesc(phaseDisp), colorbar, caxis([-4 4])
c = colorbar;
c.Label.String = 'Wavefront Error (Waves)';
set(gca,'fontsize',16)
set(gca,'XTick',[]);
set(gca,'YTick',[]);
titleString = sprintf('Simulated Corrected Wavefront Error,
Iteration #%0ld',i);
title(titleString), zlabel('Optical Effect (Waves)')
mTextBox = uicontrol('style','text');
RMSstring = sprintf('RMS = %1.3f Waves',RMS);
set(mTextBox,'String',RMSstring)
mTextBoxPosition = get(mTextBox,'Position');
set(mTextBox,'Position',[80 850 130 70])
set(mTextBox,'FontSize',14)
mTextBox2 = uicontrol('style','text');
PVstring = sprintf('PV = %1.3f Waves',PV);
set(mTextBox2,'String',PVstring)
mTextBoxPosition2 = get(mTextBox2,'Position');
set(mTextBox2,'Position',[80 800 130 70])
set(mTextBox2,'FontSize',14)
axis([0 398 0 398])
subplot(2,2,2), plot(u(:,i+1)), set(gca,'FontSize',14)

title('DM Control Voltage (V)', 'FontSize',16)
axis([0 304 -30 30]), grid on, xlabel('DM Actuators', 'FontSize',14)
ylabel('DM Actuator Voltage (V)', 'FontSize',14)
% subplot(2,2,3), imagesc(baselineDisp)
% title('Baseline Wavefront Error')

```

```
    pause(0.15)
end
```

B. CFRP ERROR CORRECTION EXPERIMENTAL MATLAB CODE

```
% LCDR Ernesto Villalba, NPS
% Program to Reduce WFE on CFRP Mirror - It requires the ESDI PC to
be
% connected via TCP/IP to the Zygo and Xinetics PCs.

% Instructions:
% Run the DMControl.m script from the Xinetics computer, wait one
second,
% then run this script.

% Credit:
% ZygoGetPhase script - Chris Wilcox, NRL
% Zernike Polynomial code (zernfun): Paul Fricker, Mathworks
% ZygoGetPhase Error checking and TCP/IP code:
% Mr. Albert Jordan, NPS and MIDN Nick D'Antonio, USNA

clear
clc

% Change to working directory
cd('Z:\PhaseData')
filedir='Z:\PhaseData\';

% Loads required data
load Index_9Oct
load Mask_9Oct
load goodIFlist_30Oct_2
load index_GoodIF_30Oct_Fix_2
load IM_9OctGCH

% Load initial commands
%load Flat_U_CMD_50Oct_1541
% load U_CMD_70Oct_test

pause(3)
% Baseline Interferometer Reading
check = 1;
while check == 1
    count=0;
    err_count=0;
    while count == err_count
        try
            [phase1] = ZygoGetPhase;
        catch MyErr
            err_count=err_count+1;
        end
        count = count+1;
    end
    prompt = 'Take another reading? Yes(1), No(0)';
```

```

    UserInput = input(prompt);
    check=UserInput;
end
% Divide Measurement by 2 for second double-pass, scale to waves and
crop,
% resize
phase1 = phase1/632.8e-9; % Scale to waves
phase1 = phase1(50:end,126:end); % crop
phase1 = (imresize(phase1,[398,398],'nearest').*Mask_9Oct); %
resize
phase1(isnan(phase1)) = 0;
check = 1;
while check == 1
    count=0;
    err_count=0;
    while count == err_count
        try
            [phase2] = ZygoGetPhase;
        catch MyErr
            err_count=err_count+1;
        end
        count = count+1;
    end
    prompt = 'Take another reading? Yes(1), No(0)';
    UserInput = input(prompt);
    check=UserInput;
end
% Divide Measurement by 2 for second double-pass, scale to waves and
crop,
% resize
phase2 = phase2/632.8e-9; % Scale to waves
phase2 = phase2(50:end,126:end); % crop
phase2 = (imresize(phase2,[398,398],'nearest').*Mask_9Oct); %
resize
phase2(isnan(phase2)) = 0;
check = 1;
while check == 1
    count=0;
    err_count=0;
    while count == err_count
        try
            [phase3] = ZygoGetPhase;
        catch MyErr
            err_count=err_count+1;
        end
        count = count+1;
    end
    prompt = 'Take another reading? Yes(1), No(0)';
    UserInput = input(prompt);
    check=UserInput;
end
% Divide Measurement by 2 for second double-pass, scale to waves and
crop,
% resize
phase3 = phase3/632.8e-9; % Scale to waves

```

```

phase3 = phase3(50:end,126:end); % crop
phase3 = (imresize(phase3,[398,398],'nearest').*Mask_9Oct); %
resize
phase3(isnan(phase3)) = 0;
% Average 3 phase measurements
phase = (phase1 + phase2 + phase3)/3;
indexNaN = find(phase == 0);
phase(indexNaN) = NaN;

% Set up Zernike theta and r variables
L = size(phase,1);
X = -1:2/(L-1):1;
[x,y] = meshgrid(X);
x = x(:); y = y(:);
[theta,r] = cart2pol(x,y);
N = []; M = [];
for n = 0:8
N = [N n*ones(1,n+1)];
M = [M -n:2:n];
end

% Remove Piston:
Phase0 = phase;
Phase0(isnan(Phase0)) = 0;
Index_PTT = find(Phase0 ~= 0);
Index_Replace = find(Phase0 == 0);
phase = phase - mean(phase(Index_PTT));

% Zernike Function:
Z = zernfun(N,M,r(Index_9Oct),theta(Index_9Oct));
%Z0 = zernfun(N,M,r(Index_PTT),theta(Index_PTT));

% Remove Tip and Tilt from Phase Measurement:
aPhase = Z\Phase0(Index_9Oct);
aPhasePTT = aPhase;
aPhasePTT(1) = 0;
aPhasePTT(4:length(aPhase)) = 0; % set all
others to zero
PhasePTT = NaN(size(Phase0));
PhasePTT(Index_9Oct) = Z*aPhasePTT;
phase = (phase - PhasePTT).*Mask_9Oct;
phaseDisp = phase;
baselineDisp = phase;
phase(isnan(phase)) = 0;
Index_RMS = find(phase ~= 0);

% % Replace zeros with Zernike Estimation:
% PhaseReplace = NaN(size(Phase0));
% PhaseReplace(Index_9Oct) = Z*aPhase;
% PhaseReplace(isnan(PhaseReplace)) = 0;
% PhasePTT(isnan(PhasePTT)) = 0;
% PhaseReplace = PhaseReplace - PhasePTT;
% PhaseReplace = PhaseReplace - mean(PhaseReplace(:));
% Index_replace = find(Phase0 == 0);

```

```

% PhaseReplaceAdd = zeros(398,398);
% PhaseReplaceVec = PhaseReplace(Index_replace);
% PhaseReplaceAdd(Index_replace) = PhaseReplaceVec;
% phase = phase + PhaseReplaceAdd;

phaseVec = phase(Index_9Oct); % Phase data to
vector format
phaseVecRMS = phase(Index_RMS);
%RMS = rms(phase(:));
RMS = rms(phaseVecRMS);
baseline = phase;
baselineVec = baseline(Index_RMS);
%baselineRMS = rms(baseline(:));
baselineRMS = rms(baselineVec);
% Save baseline measurement for future reference
filename=sprintf('%sBaseline%s.mat',filedir,datestr(now,'dd-mmm-
YYYY_HHMM'));
save(filename, 'baselineDisp')

%% Control Loop - Corrects WFE % Number of control
m = 70; iterations
u = zeros(length(goodIFlist_30Oct_2),m);
%u(:,1) = Flat_U_CMD_50Oct_1541;
%u(:,1) = U_CMD_70Oct_test;
uCount = zeros(length(goodIFlist_30Oct_2),m);
uCountMatrix = zeros(21,21);
uCountMatrixRec = zeros(21,21,m);
Gain = 0.1;
% Calculate voltage range of IM measurements
count = 800;
Volt_perCount = 14.65/1000; % V
VoltageRef = count*Volt_perCount;

figure(1)
subplot(2,2,1), imagesc(phaseDisp), colorbar
titleString = sprintf('Residual WFE, Iteration #01d',i);
title(titleString), xlabel('Optical Effect (Waves)')
mTextBox = uicontrol('style','text');
RMSstring = sprintf('RMS = %1.3f Waves',RMS);
set(mTextBox, 'String',RMSstring)
mTextBoxPosition = get(mTextBox, 'Position');
set(mTextBox, 'Position', [50 600 100 40])
set(mTextBox, 'FontSize', 12)

subplot(2,2,2), plot(u(:,1)), grid
title('Control Voltage (V)')
axis([0 304 -30 30])

subplot(2,2,3), imagesc(baselineDisp), colorbar
title('Baseline WFE')
BaselineRMSstring = sprintf('RMS = %1.3f Waves',baselineRMS);
pTextBox = uicontrol('style','text');
set(pTextBox, 'String',BaselineRMSstring)

```

```

pTextBoxPosition = get(pTextBox, 'Position');
set(pTextBox, 'Position', [50 50 100 40])
set(pTextBox, 'FontSize', 12)

% Optimization Parameters
u_max = (30*ones(304,1))/VoltageRef;    % scaled units
u_min = (-30*ones(304,1))/VoltageRef;  % scaled units
u_ub = zeros(304,1);
u_lb = zeros(304,1);
%   A_bound = eye(304);
%   b_bound = ones(304,1)*(20/VoltageRef);
filedir='Z:\PhaseData\';
for i = 1 : m
% Generate control commands in Volts:
% Compute upper and lower bounds (available control authority)
u_prev = (u(:,i))/VoltageRef;          % scaled units
u_ub = u_max - u_prev;                 % scaled units
u_lb = u_min - u_prev;                 % scaled units

    u_opt = lsqlin(IM_9OctGCH, phaseVec, [], [], [], [], u_lb, u_ub, u_prev); %
scaled units
    u_delta = Gain*(u_opt.*VoltageRef); % in Volts
    u(:,i+1) = u(:,i) - u_delta;        % in Volts
    for ii = 1 : length(index_GoodIF_30Oct_Fix_2)
        if u(ii,i+1) >= 30              % sets max voltage at
20 V
            u(ii,i+1) = 30;
        elseif u(ii,i+1) <= -30         % sets min voltage at -
20 V
            u(ii,i+1) = -30;
        end
    end
end

pause(1)
% Verifies that the DM map is set on the Xinetics computer
tcpipClient2=tcip('169.254.214.248',3000,'NetworkRole','Client');
set(tcpipClient2,'InputBufferSize',500);
set(tcpipClient2,'OutputBufferSize',500);
set(tcpipClient2,'Timeout',15);
fopen(tcpipClient2);
inputcheck=fread(tcpipClient2,1,'double');
fclose(tcpipClient2);

subplot(2,2,2), plot(u(:,i+1)), grid on
title('Control Voltage (V)')
axis([0 length(goodIFlist_30Oct_2) -30 30])
% Pause to evaluate voltage command
%pause()

% Control in "counts"
uCount(:,i+1) = u(:,i+1)/Volt_perCount;
uCount(:,i+1) = round(uCount(:,i+1));
uCountMatrix(index_GoodIF_30Oct_Fix_2) = uCount(:,i+1);
uCountMatrixRec(:, :, i+1) = uCountMatrix;

```

```

% Send control input to Xinetics computer
if count>err_count

dlmwrite('DM_Flat.csv',uCountMatrixRec(:, :, i+1), 'delimiter', ',', 'newline', 'pc')
    type DM_Flat.csv
    outputcheck=1;
    s=whos('outputcheck');
    tcpipServer=tcpip('0.0.0.0',3000, 'NetworkRole', 'Server');
    set(tcpipServer, 'OutputBufferSize', s.bytes)
    fopen(tcpipServer);
    fwrite(tcpipServer,outputcheck(:), 'double');
end

% Take next Interferometer Measurement
pause(3)
check = 1;
while check == 1
count=0;
err_count=0;
while count == err_count
try
    [phase1] = ZygoGetPhase;
catch MyErr
    err_count=err_count+1;
end
count = count+1;
end
prompt = 'Take another reading? Yes(1), No(0)';
UserInput = input(prompt);
check=UserInput;
end
% Divide Measurement by 2 for second double-pass, scale to waves
and crop,
% resize
phase1 = phase1/632.8e-9; % Scale to
waves
phase1 = phase1(50:end,126:end); % crop
phase1 = (imresize(phase1,[398,398], 'nearest')).*Mask_90Oct);
% resize
phase1(isnan(phase1)) = 0;
check = 1;
while check == 1
count=0;
err_count=0;
while count == err_count
try
    [phase2] = ZygoGetPhase;
catch MyErr
    err_count=err_count+1;
end
count = count+1;
end
prompt = 'Take another reading? Yes(1), No(0)';

```

```

    UserInput = input(prompt);
    check=UserInput;
    end
    % Divide Measurement by 2 for second double-pass, scale to waves
and crop,
    % resize
    phase2 = phase2/632.8e-9; % Scale to
waves
    phase2 = phase2(50:end,126:end); % crop
    phase2 = (imresize(phase2,[398,398],'nearest').*Mask_9Oct);
% resize
    phase2(isnan(phase2)) = 0;
    check = 1;
    while check == 1
        count=0;
        err_count=0;
        while count == err_count
            try
                [phase3] = ZygoGetPhase;
            catch MyErr
                err_count=err_count+1;
            end
            count = count+1;
        end
        prompt = 'Take another reading? Yes(1), No(0)';
        UserInput = input(prompt);
        check=UserInput;
    end
    % Divide Measurement by 2 for second double-pass, scale to waves
and crop,
    % resize
    phase3 = phase3/632.8e-9; % Scale to
waves
    phase3 = phase3(50:end,126:end); % crop
    phase3 = (imresize(phase3,[398,398],'nearest').*Mask_9Oct);
% resize
    phase3(isnan(phase3)) = 0;
    % Average 3 phase measurements
    phase = (phase1 + phase2 + phase3)/3;
    indexNaN = find(phase == 0);
    phase(indexNaN) = NaN;

    % Remove Piston, Tip and Tilt from Phase Measurement:
    Phase0 = phase;
    Phase0(isnan(Phase0)) = 0;
    Index_PTT = find(Phase0 ~= 0);
    phase = phase - mean(phase(Index_PTT));

    aPhase = Z\Phase0(Index_9Oct);
    aPhasePTT = aPhase;
    aPhasePTT(1) = 0;
    aPhasePTT(4:length(aPhase)) = 0; % set all
others to zero
    PhasePTT = NaN(size(Phase0));

```

```

PhasePTT(Index_9Oct) = Z*aPhasePTT;
phase = (phase - PhasePTT).*Mask_9Oct;
phaseDisp = phase;
phase(isnan(phase)) = 0;
Index_RMS = find(phase ~= 0);

%      % Replace zeros with Zernike Estimation:
%      PhaseReplace = NaN(size(Phase0));
%      PhaseReplace(Index_9Oct) = Z*aPhase;
%      Index_replace = find(Phase0 == 0);
%      PhaseReplaceAdd = zeros(398,398);
%      PhaseReplaceVec = PhaseReplace(Index_replace);
%      PhaseReplaceAdd(Index_replace) = PhaseReplaceVec;
%      phase(isnan(phase)) = 0;
%      phase = phase + PhaseReplaceAdd;

phaseVec = phase(Index_9Oct); % Phase data to
vector format
phaseVecRMS = phase(Index_RMS);
%RMS = rms(phase(:));
RMS = rms(phaseVecRMS);

% Display results:
subplot(2,2,1), imagesc(phaseDisp), colorbar
titleString = sprintf('Residual WFE, Iteration %01d',i);
title(titleString), xlabel('Optical Effect (Waves)')
mTextBox = uicontrol('style','text');
RMSstring = sprintf('RMS = %1.3f Waves',RMS);
set(mTextBox,'String',RMSstring)
mTextBoxPosition = get(mTextBox,'Position');
set(mTextBox,'Position',[50 600 100 40])
set(mTextBox,'FontSize',12)

filename=sprintf('%sInterim_phase%03d.mat',filedir,i);
save(filename,'phaseDisp')
filename=sprintf('%sInterim_control%03d.mat',filedir,i);
u_interim = u(:,i);
save(filename,'u_interim')
end

filename=sprintf('%sCorrectedPhase%s.mat',filedir,datestr(now,'dd-mmm-
yyyy_HHMM'));
save(filename,'phaseDisp')
filename=sprintf('%su_control%s.mat',filedir,datestr(now,'dd-mmm-
yyyy_HHMM'));
save(filename,'u')

```

THIS PAGE INTENTIONALLY LEFT BLANK

LIST OF REFERENCES

- [1] B. N. Agrawal, “Research proposal: Large aperture and cost-effective primary space mirrors, FY15,” unpublished.
- [2] R. C. Romeo and R. N. Martin, “Progress in 1m-class lightweight CFRP composite mirrors for the ULTRA Telescope,” in *Proc of SPIE*, 2006, vol. 6273, pp. 70184D-1–70184D-11.
- [3] R. C. Romeo, “CFRP composites for optics and structures in telescope applications,” in *Proc. of SPIE*, 1995, vol. 2543, pp. 154–161.
- [4] J. J. Kim, M. Allen and B. Agrawal, “Cost-effective aperture with deformable mirror for imaging satellites,” presented at the 66th International Astronautical Conference, Jerusalem, Israel, 2015.
- [5] B. N. Agrawal, Jae-Jun Kim and M. Allen, “Cost-effective large apertures for future imaging satellites,” presented at the *AIAA SPACE Conference*, Pasadena, CA, 2015, vol. 4494.
- [6] R. K. Tyson, *Principles of Adaptive Optics*, 3rd ed. Boca Raton, FL: CRC Press, 2011.
- [7] J. R. Andrews, S. R. Restaino, T. Martinez, C. C. Wilcox, F. Santiago, S. Teare, R. Romeo, R. Martin and D. Wick, “Prototype 0.4 meter carbon fiber reinforced polymer (CFRP) telescope: specifications and initial testing,” in *Proc. of SPIE*, 2008, vol. 7018, pp. 62730S-1 - 62730S-12.
- [8] B. Baldauf, T. Magaldi, R. Matijevich, T. Bruno and J. Vayda, “Actuated carbon fiber reinforced polymer mirror development,” unpublished.
- [9] Peak-to-Valley vs. RMS. (n.d.). Diffraction limited. [Online]. Available: http://www.cyanogen.com/help/quickfringe/QUICK_FRINGEPeaktoValley_vs_RMS.htm.
- [10] Root-Mean-Square. (n.d.). Wolfram MathWorld. [Online]. Available: <http://mathworld.wolfram.com/Root-Mean-Square.html>.
- [11] R. K. Tyson and B. W. Frazier, *Field Guide to Adaptive Optics*, 2nd ed. Bellingham, WA: SPIE Press, 2012.
- [12] Xinetics Inc., *Deformable Mirror High Voltage Amplifier System User Manual*, unpublished.

- [13] B. R. Oppenheimer, D. L. Palmer, R. G. Dekany, A. Sivaramakrishnan, M. A. Ealey and T. R. Price, “Investigating a Xinetics Inc. deformable mirror,” *SPIE*, vol. 3126, pp. 569–579, 1997.
- [14] Surface Normal Mirrors. (n.d.). Northrup Grumman. [Online]. Available: <http://www.northropgrumman.com/BusinessVentures/AOAXinetics/IntelligentOptics/Products/Pages/SurfaceNormalMirrors.aspx>.
- [15] Xinetics Inc, *Deformable Mirror High Voltage Amplifier System WinHVA Software User Manual*, unpublished.
- [16] GPI XP, GPI XPHR, GPI HS specifications. (n.d.). Zygo Corporation. [Online]. Available: http://www.lambdaphoto.co.uk/pdfs/GPI_xp_spec.pdf.
- [17] M. R. Allen, “Wavefront control for space telescope applications using adaptive optics,” M.S. thesis, MAE, Naval Postgraduate School, Monterey, CA, 2007.
- [18] J. J. Watson, “Correcting Surface Figure Error in Imaging Satellites Using a Deformable Mirror,” M.S. thesis, MAE, Naval Postgraduate School, Monterey, CA, 2013.
- [19] S. Boyd and L. Vandenberghe, “Vectors, matrices, and least squares (Working Title),” unpublished.
- [20] MATLAB documentation—LSQLIN function. (n.d.). MathWorks. [Online]. Available: <http://www.mathworks.com/help/optim/ug/lsqlin.html>.
- [21] B. N. Agrawal, “Research proposal: Cost-effective large aperture imaging satellites, FY16,” unpublished.

INITIAL DISTRIBUTION LIST

1. Defense Technical Information Center
Ft. Belvoir, Virginia
2. Dudley Knox Library
Naval Postgraduate School
Monterey, California